Aus der Berlin Ultrahigh Field Facility (B.U.F.F.) am
Max-Delbrück-Centrum (MDC) für Molekulare Medizin in der
Helmholtz Gemeinschaft, Berlin-Buch

DISSERTATION

Radiofrequency induced heating for controlled release of a load from thermoresponsive carriers: a 7.0 Tesla Thermal Magnetic Resonance Study

Radiofrequenz induzierte und kontrollierte Freisetzung einer Ladung aus thermoreaktiven Trägern: Thermale Magnetresonanz bei 7.0 Tesla

zur Erlangung des akademischen Grades
Doctor rerum medicinalium (Dr. rer. medic.)

vorgelegt der Medizinischen Fakultät
Charité – Universitätsmedizin Berlin

von

Yiyi Ji

aus Qingtian, Zhejiang, China

Datum der Promotion: 18. September 2020

Contents

List of abbreviations and symbols 4

List of Images 5

Abstract 6

Zusammenfassung 8

1. Introduction 10

1.1. Thermal magnetic resonance 10

1.2. Temperature controlled load release 12

1.3. Goal of this doctoral work 13

2. Materials and Methods 14

2.1. Transmit and Receive Tx/Rx switch 14

2.1.1. Circuit design 14

2.1.2. MR imaging test 15

2.1.3. RF induced heating and MR thermometry 16

2.2. Load release from thermoresponsive carriers 17

2.2.1. Synthesis and characterization of thermoresponsive nanogels 17

2.2.2. Protein encapsulation in the thermoresponsive nanogels 18

2.2.3. Protein Release study in water bath 19

2.2.4. Phantom design for radiofrequency induced heating in an MR scanner 19

2.2.5. Experimental setup for radiofrequency induced heating in an MR scanner 21

2.2.6. Radiofrequency induced heating paradigm and protein release study 23

3. Results 24

3.1. High-power Tx/Rx switch 24

3.1.1. Tx/Rx switch performance 24

3.1.2. MR imaging test 25
3.1.3. RF induced heating and MR thermometry 25
3.2. Load release from thermoresponsive carriers 27
3.2.1. Thermoresponsive nanogel characterization 27
3.2.2. Protein release from nanogel: in water bath 28
3.2.3. Temperature simulations of the phantom 29
3.2.4. RF heating of the phantom 30
3.2.5. Protein release from nanogel: Thermal MR 30
4. Discussion and Conclusion 33
5. References 36
Statutory Declaration 39
Declaration of own contribution 40
Publication: Ji Y, Hoffmann W, Pham M, Dunn AE, Han H, Oezerdem C, Waiczies H, Rohloff M, Endemann B, Boyer C, Lim M, Niendorf T and Winter L, “High peak and high average radiofrequency power transmit/receive switch for thermal magnetic resonance.” Magn. resonance in medicine (2018). DOI: 10.1002/mrm.27194. 41
Curriculum Vitae 52
List of Publications 56
Acknowledgments 59

List of abbreviations and symbols

λ	Wavelength
Ac-dPG	Acrylated dendritic polyglycerol
B_0	Static magnetic field
BSA	Bovine serum albumin
BSA-FITC	Bovine serum albumin labelled with fluorescein
EM	Electromagnetic
f	Frequency
MR	Magnetic resonance
MRI	Magnetic resonance imaging
MRTh	Magnetic resonance thermometry
P_{avg}	Average power
PIN	Positive-intrinsic-negative
PNIPAM	Poly(N-isopropylacrylamide)
PNIPMAM	Poly(N-isopropyl methacrylamide)
PTFE	Polytetrafluoroethylene
RF	Radio-frequency
T	Tesla
Thermal MR	Thermal magnetic resonance
Tx/Rx	Transmit/receive
UHF	Ultrahigh field
VPTT	Volume phase transition temperature
W	Watt

List of Images

Figure 1 – Thermal magnetic resonance. 11

Figure 2 – Schematics of drug release from a thermoresponsive nanogel 13

Figure 3 – Circuit diagram of the high power Tx/Rx switch 14

Figure 4 – Constructed high-power Tx/Rx switch 15

Figure 5 – RF heating setup in the MR scanner 16

Figure 6 – Agarose phantom and the setup for the electromagnetic field and temperature simulations 20

Figure 7 – RF heating setup for the MR scanner for temperature controlled protein release from thermoresponsive nanogels 22

Figure 8 –Temperature in the circuit of high power and conventional Tx/Rx switch when driving P_{avg} = 100 W 24

Figure 9 – Wrist MRI performed with high power and conventional Tx/Rx switch 25

Figure 10 – RF heating with high-power Tx/Rx switch (P_{avg} = 100 W) vs conventional Tx/Rx switch (P_{avg} = 25 W) 26

Figure 11 – NMR spectra of acrylated dendritic polyglycerol (Ac-dPG) and the nanogels and the graph of volume phase transition temperature (VPTT) 27

Figure 12 – Bovine saline albumin labelled with fluorescein (BSA-FITC) release from the nanogels using water bath as heat source 28

Figure 13 – Simulated radiofrequency induced heating in the phantom with P_{avg} = 100 W for 15 minutes 29

Figure 14 – Temperature distribution maps in the phantomn obtained with MR thermometry 31

Figure 15 – Bovine serum albumin labelled with fluorescein (BSA-FITC) released from the nanogels using RF heating from thermal MR 32

Abstract

Introduction

Temperature is an important attribute of life. Radiofrequency (RF) pulses used for magnetic resonance (MR) spin excitation can be deliberately used to apply a thermal stimulus. Thermal MR integrates this thermal modulation with the imaging capabilities of a MR device providing a tool to study the role of temperature in biological systems, diagnostic contrasts and thermal therapies (e.g. temperature controlled release of a load from thermoresponsive carriers).

Thermal MR requires an RF chain that includes dedicated transmit/receive (Tx/Rx) switches that support high peak powers for MR imaging and high average powers for RF heating. Conventional Tx/Rx switches have electronic components in the transmission path limiting the average power handling. In this work, a high power handling Tx/Rx switch design is developed, implemented, and evaluated. This technology was applied in a pilot study in humans and in a feasibility study demonstrating the proof-of-principle of Thermal MR for temperature controlled release of a protein from thermoresponsive nanogels.

Methods

In the Tx/Rx switch design, λ/4 stubs were used to route the transmitted RF signal directly to the RF coil/antenna without passing through any electronic components (e.g. PIN diodes). Bench measurements, MR imaging, MR thermometry, and RF heating experiments were performed at f=297MHz (B_0=7T) to examine the characteristics and applicability of the switch.

Bovine serum albumin (BSA) was loaded to thermoresponsive nanogels (transition temperature = 38°C). As a reference, the release rate was firstly accessed using water bath heating at temperatures: 20°C, 37°C and 43°C. BSA release from the nanogel was subsequently studied using RF heating of Thermal MR at the same temperatures. In this Thermal MR setup one bow tie dipole antenna and a dedicated phantom were used.

Results

The proposed design for the Tx/Rx switch provided 35.7dB/41.5dB (Tx/Rx) of isolation and 0.41dB/0.27dB (Tx/Rx) of insertion loss. The switch supported high peak (3.9kW) and high average (120W) RF powers for MRI and RF heating. High-resolution MRI of the wrist yielded image quality competitive with that obtained with a conventional Tx/Rx switch. RF heating in phantom monitored by MR thermometry demonstrated the switch applicability for thermal modulation.

The release of BSA from the thermoresponsive nanogels after 6 hours was 12.5% (20°C), 19.5% (37°C) and 32.8% (43°C) in water bath and 12.9% (20°C), 19.6 (37°C) and 29.3% (43°C) with Thermal MR.

Conclusion

The high-power Tx/Rx switch enables thermal MR applications at 7.0 Tesla. The reference release profile of the therapeutic load model from the nanocarrier obtained with a water bath setup used for temperature intervention is in accordance with the release kinetics deduced from the thermal MR setup. This finding supports the feasibility of thermal MR for temperature controlled release of a load from thermoresponsive nanocarriers.

Zusammenfassung

Einleitung

Temperatur ist eine physikalische Größe und wichtige Eigenschaft biologischer Systeme. Hochfrequenzimpulse zur Spinanregung in der Magnetresonanztomographie (MRT) können gezielt zur Erzeugung eines thermischen Stimulus eingesetzt werden (Thermale MR, tMR). Die tMR verbindet eine solche thermische Modulation mit der MRT und stellt somit ein Werkzeug zur Untersuchung der Rolle von Temperatur in biologischen Systemen, zur Darstellung diagnostischer Kontraste, sowie zur Therapie (z.B. durch kontrollierte Freisetzung einer Ladung von thermoreaktiven Trägern) dar. Allerdings benötigt die tMR eine HF-Kette mit speziellen Sende/Empfangsschaltern (Tx/Rx), welche sowohl hohe Spitzenleistungen für die MRT, als auch hohe Durschnittsleistungen für die thermische Stimulation zulassen. Letztere Anforderung wird durch konventionelle Tx/Rx Schalter nicht erfüllt. Zur Lösung wurde in dieser Arbeit ein neues Tx/Rx Schalterdesign entwickelt, implementiert und evaluiert. Die entwickelte HF-Technologie wurde in einer Human-Pilotstudie zur Anwendung geführt. Zusätzlich wurde sie in einer Machbarkeitsstudie an Messphantomen eingesetzt, um die kontrollierte Freisetzung eines Proteins aus einem thermoreaktiven Nanogel mittels tMR zu demonstrieren.

Methoden

Im entwickelten Tx/Rx Schalter wurden λ/4 Stichleitungen integriert, um das HF-Signal direkt zur HF-Antenne zu leiten, ohne durch elektronische Komponenten (z.B. PIN Dioden) zu gelangen. Alle Experimente (MRT, MR-Thermometrie und HF Erwärmung) wurden bei einer Frequenz von 297MHz (B_0=7.0T) durchgeführt, um die Eigenschaften des Schalters zu untersuchen.

Ein thermoreaktives Nanogel (Übergangstemperatur=38°C) wurde mit Rinderserumalbumin (BSA) beladen. Als Referenz diente die Freisetzungskinetik im Wasserbad bei Temperaturen von 20°C, 37°C und 43°C. Die BSA Freisetzung durch HF Erwärmung mit tMR wurde bei den selben Temperaturen gemessen.

Hierfür wurden eine Dipol-HF-Antenne und ein entsprechendes Phantom verwendet.

Ergebnisse

Der entworfene Tx/Rx Schalter führte zu eine Isolierung von 35.7dB/41.5dB und einer Dämpfung von 0.41dB/0.27dB während des Sendens/Empfangens. Der Schalter ermöglichte hohe Spitzen- (3.9kW) und Durchschnittsleistungen (120W) für MRT und tMR. Hochaufgelöste MRT-Bilder des Handgelenks zeigten eine Bildqualität vergleichbar mit Aufnahmen eines konventionellen Tx/Rx Schalters. Die durch tMR induzierte Erwärmung des Phantoms demonstrierte die Eignung des Schalters für thermische Modulation. Die BSA-Freisetzung betrug nach 6 Stunden 12,5% (20°C), 19,5% (37°C) und 32,8% (43°C) im Wasserbad und 12,9% (20°C), 19,6% (37°C) und 29,3% (43°C) mit tMR.

Fazit

Der entwickelte Hochleistungs-Tx/Rx-Schalter ermöglicht tMR bei 7.0T. Das Freisetzungsprofil der im Wasserbad gemessen Referenzdaten stimmt mit der durch tMR erzeugten Freisetzungskinetik überein. Diese Ergebnisse demonstrieren die Realisierbarkeit einer kontrollierten Freisetzung der Ladung von thermoreaktiven Nanoträgern durch thermale MR.

1. Introduction

Part of this thesis is based on the work published on Ji et al. 2018 [1]; therefore, it contains direct passages from this publication.

Temperature is a physical parameter with diverse biological implications [2] and strong clinical interest. Therapies with thermal intervention include thermal ablation (<60 °C) for neurosurgery [3], hyperthermia (41-45 °C) as adjuvant treatment to chemo- and radiotherapies [4], and temperature controlled drug release [5].

All the thermal interventions need an anatomical reference to localize the target site to apply the heat, temperature monitoring to assure the correct amount of heat is delivered (too high temperatures can burn the tissue, while too low temperatures might not achieve desired therapeutic effect), and a source to deliver the heat. Here the magnetic resonance system is a valuable tool, as it provides high tissue contrast anatomical images, non-invasive temperature monitoring by means of magnetic resonance thermometry (MRTh), and the radiofrequency (RF) pulses tailored for spin excitation for imaging can also be used for the application of a thermal stimulus [6]. The addition of a thermal modulation to magnetic resonance imaging is denoted as thermal magnetic resonance – thermal MR.

1.1. Thermal magnetic resonance

The radiofrequency pulses used in magnetic resonance imaging are electromagnetic waves with an electric and a magnetic field components. While the magnetic field is used for imaging, the electric field power can be absorbed by the tissue and cause temperature rise. The tissue heating is considered an undesired side effect of MRI and regulatory organizations such as the International Electrotechnical Commission (IEC) restrict the maximum input power of RF to assure patient safety [7].

At ultrahigh field magnetic resonance (UHF-MR, $B_0 \geq 7.0$ T, f ≥ 300 MHz), the shortening of the radiofrequency (RF) wavelength in tissue gives rise to high focusing of RF fields due to constructive interference [6,8]. Contrary to the notion that this phenomenon is considered an adverse outcome, the potential to focus radiofrequency (RF) energy onto a small target region can be translated into localized power deposition, a means for targeted RF induced temperature modulation. This approach, denoted as Thermal MR (**Figure 1**), uses the pulsed power amplifier of the MR system together with dedicated RF antenna arrays to generate RF induced focal thermal modulation in combination with higher signal-to-noise ratio imaging capabilities of UHF-MR.

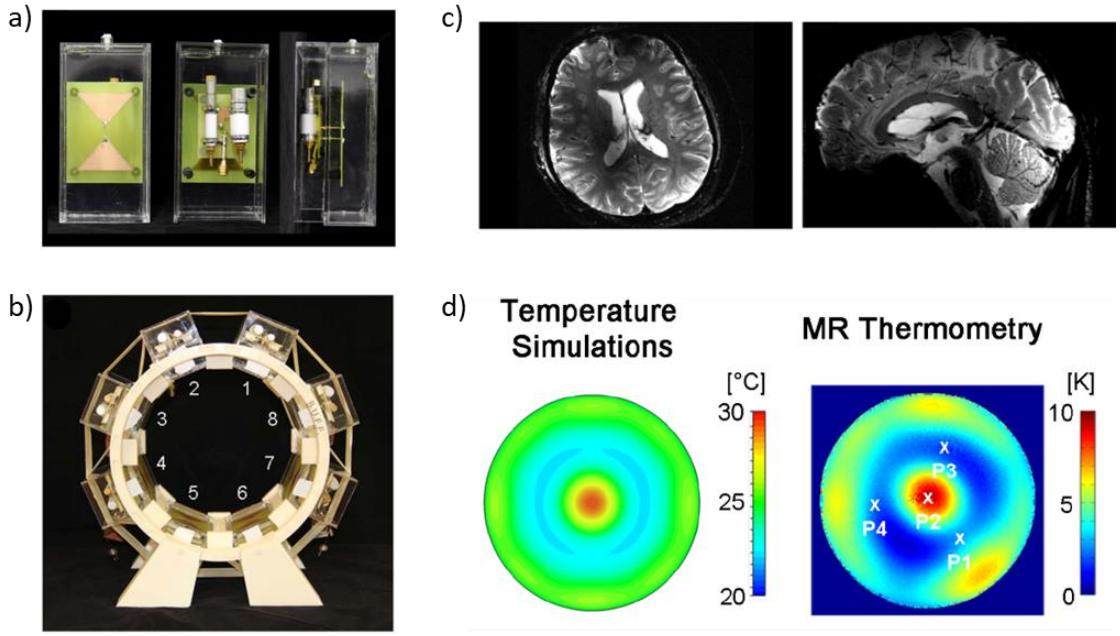

Figure 1 – Thermal magnetic resonance. **a)** Photograph of a bow tie dipole RF antenna building block. **b)** Thermal MR applicator with eight bow tie antenna RF antennae. **c)** MR images of a brain acquired with Thermal MR applicator. **d)** Temperature simulation and MR thermometry showing the hotspot created by Thermal MR applicator in the middle of a phantom. Image adapted from [6].

Performing MRI and RF heating simultaneously requires high peak power (>1 kW) and high average power (100 W per channel), support of the RF antennae as well as other RF hardware components. While RF antennae have already been developed for thermal MR, high peak and high average RF power

transmit/receive (Tx/Rx) switches – that alternate between high power (kW) transmission to low power (μW) reception of the RF signal – are still lacking.

Magnetic resonance Tx/Rx switches deploy positive-intrinsic-negative (PIN) diodes as active switching units, as they offer very low resistance in forward biased state, high isolation in the reverse bias state, fast switching time and high peak power handling. In conventional Tx/Rx switch designs, PIN diodes are directly in the transmission pathway, limiting the average power handling (e.g. at high duty cycles). Thus, the overall applicable average power is limited severely in order to avoid excessive heat accumulation in these components. A Tx/Rx switch design that route transmitted RF signal directly to the RF antenna without electronic components on the transmission path would handle higher power RF pulses.

1.2. Temperature controlled load release

The delivery of therapeutics to its target site is a crucial requirement for a successful treatment. The lack of specificity in the current delivery of drug formulations can cause systemic side effects and/or have a low available therapeutic dose at the target [9–11]. To address these shortcomings, nanotechnology has played an important role in smart delivery of drugs, contrast agents, genes, proteins, etc. [12–15]. One of the novel delivery methods is based on stimulus-responsive smart carriers that deliver their load upon one or more stimuli [16–18]. Such stimuli can be internal, related to changes in the microenvironment of certain diseases (pH variations, hormone concentrations, redox gradient, etc.), or external such as heat, light or magnetic field [14,19]. The temperature stimulus is particularly interesting as it can be externally applied and thus be spatially and temporally controlled including reaching deep lying tissues [20–22].

There are many formulations for thermoresponsive carriers: liposomes [15,23], polymers [5,20], nanogels [24] and many others. All of them present a sharp phase transition upon reaching a transition temperature and consequently, release their load (e.g. a drug or a contrast agent, **Figure 2**). In this way, the drug

is only released on the heated target site, avoiding systemic toxicity and increasing therapeutic dose.

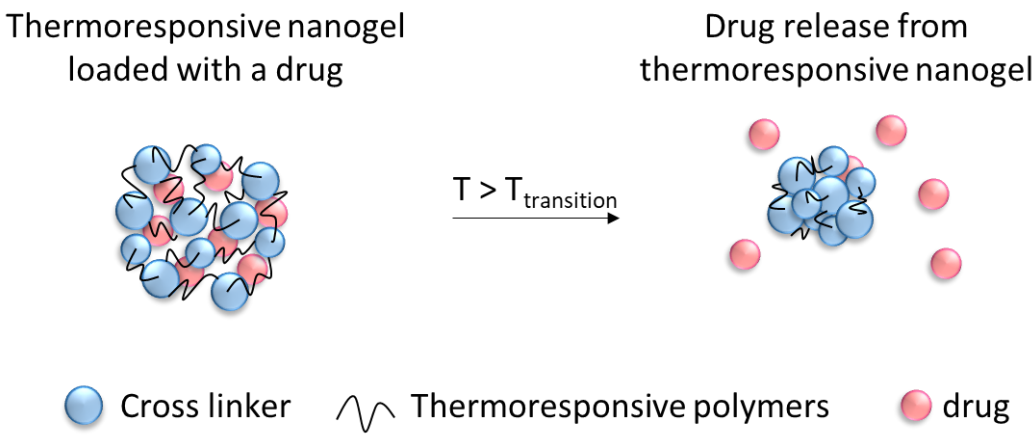

Figure 2 – Schematics of drug release from a thermoresponsive nanogel upon reaching its transition temperature. Courtesy of Dr. Lucila Navarro, Freie Universität Berlin.

1.3. Goal of this doctoral work

The goal of this doctoral work is firstly to develop a new design for a high power Tx/Rx switch that can perform MR imaging, comparable to conventional switches, and at same time, handle high power demands required for RF heating in a 7.0 Tesla magnetic resonance system. With the developed high power Tx/Rx switch, the second goal of this work is to demonstrate the feasibility of using radiofrequency heating of thermal MR for temperature triggered load release from thermoresponsive carriers.

2. Materials and Methods

2.1. Transmit and Receive Tx/Rx switch

2.1.1. Circuit design

The circuit of the proposed Tx/Rx switch is shown in **Figure 3**. It consisted of 3 quarter wavelength (λ/4) stubs and two pin diodes (MA4P7441F-1091T, Macom, MA, USA): D1 and D2. An LC resonant circuit tuned to 297 MHz (7.0 Tesla) is placed between each pin diode and λ/4 stub to afford maximum isolation between transmission (Tx) and receive (Rx) paths. The LC resonant circuits were placed in double shielded compartments to increase isolation (Tx and Rx compartments). A copper plate with 2.5 x 4 mm^2 and 2 mm of thickness was placed under each pin diodes for heat dissipation (**Figure 4**). The λ/4 stubs were assembled with semi-rigid coaxial cable (Sucoform 141 Cu 50 Ω, Huber+Suhner AG, Herisau, Switzerland) for 297 MHz.

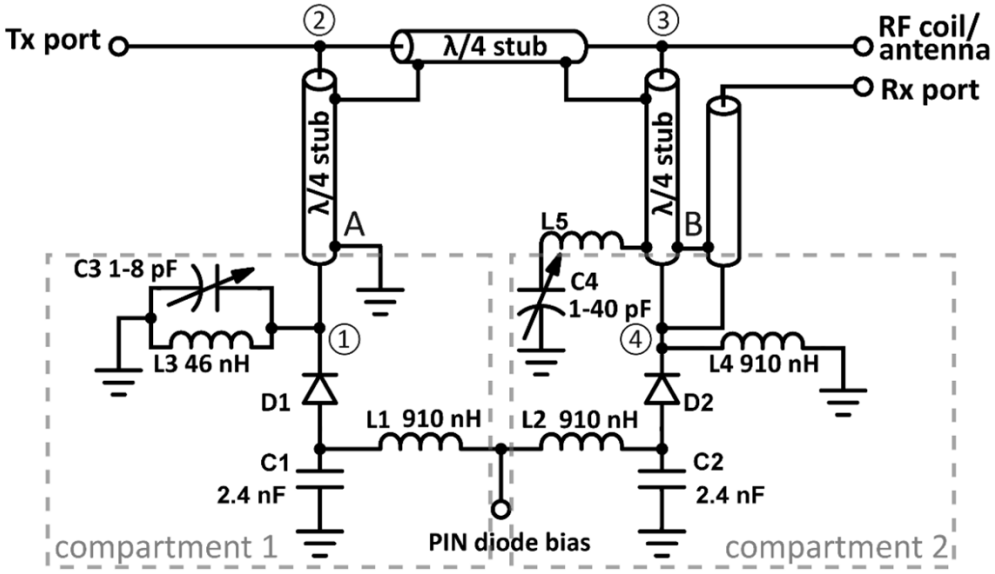

Figure 3 – Circuit diagram of the high power Tx/Rx switch. Image adapted from [1].

During the transmission mode, the pin diodes are forward biased. The low impedance at points 1 and 4 (**Figure 3**) is transformed into high impedance at points 2 and 3 by the λ/4 stubs. In this way, all RF signal from Tx port is routed into the RF coil.

During the receive mode, the pin diodes are reverse biased. The high impedance at point 4 is transformed in low impedance at point 3 and again in high impedance at point 2 by the λ/4 stubs, directing the received signal from the antenna into the receive port.

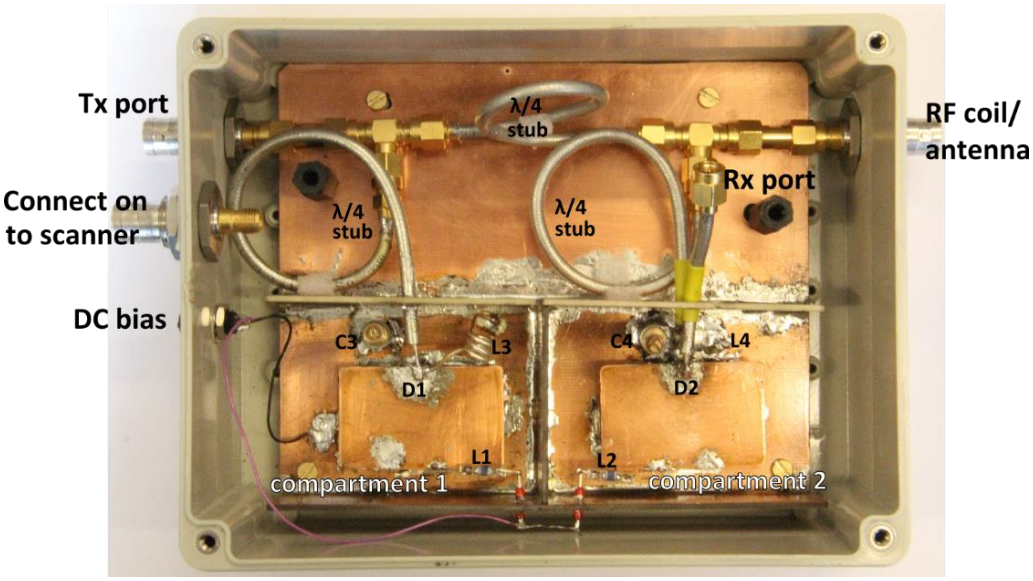

Figure 4 – Constructed high-power Tx/Rx switch. Image adapted from [1].

The isolation and insertion loss of the high-power Tx/Rx switch were accessed by measuring scattering parameters (S-parameters) using a vector network analyzer (ZVT 8, Rhode & Schwarz, Memmingen, Germany).

The power handling of the switch was tested by applying an average power (P_{avg}) of 100 W. The power was generated by an MR RF power amplifier (8 kW peak power, 4 ms rectangular pulse, U = 332 V) with a duty cycle of 10%. As reference, a conventional Tx/Rx switch (Stark Contrasts, Erlangen, Germany) used for MR imaging at 7.0 T was also submitted to the same average power. The temperature of both switches while operating at 100 W was monitored with an infrared camera (Ti25, Fluke, WA, USA).

2.1.2. MR imaging test

To test the suitability of the high-power Tx/Rx switch for MR imaging, we performed MRI on a human wrist in a B_0 = 7.0 T whole body MR system

(Magnetom, Siemens Healthcare, Erlangen, Germany) using one bow tie dipole antenna for transmission and reception of RF signal. A rapid acquisition with refocused echoes (RARE) technique was used; in plane resolution = (0.3 × 0.3) mm^2, slice thickness = 3 mm, matrix size = (320 × 320) mm^2, number of slices = 11, TR = 3000 ms, TE = 59 ms, nominal flip angle = 150°, reference transmitter voltage = 250 V, total scan time = 149 s. As reference, a conventional Tx/Rx switch was used in the same setup for image quality comparison.

2.1.3. RF induced heating and MR thermometry

An experimental setup comprising a rectangular agarose phantom (90 × 180 × 260 mm^3) and a bow tie dipole antenna [4] (**Figure 5a**) was used to examine the suitability of the high-power Tx/Rx switch for RF heating in a B_0 = 7.0 T MR system and also for temperature monitoring using MR thermometry (MRTh). The agarose phantom (σ = 1.12 S/m, ε_r = 84.4) had seven cylindrical sample holders; five were located in the RF heating range of a dipole antenna and two were located outside the heating range, **Figure 5b**. 1 mm tubes were inserted along the long axis of the phantom at depth of 5, 15, 25 and 35 mm (**Figure 5c**) for accommodating fiber optic probes that were used as temperature reference for MRTh.

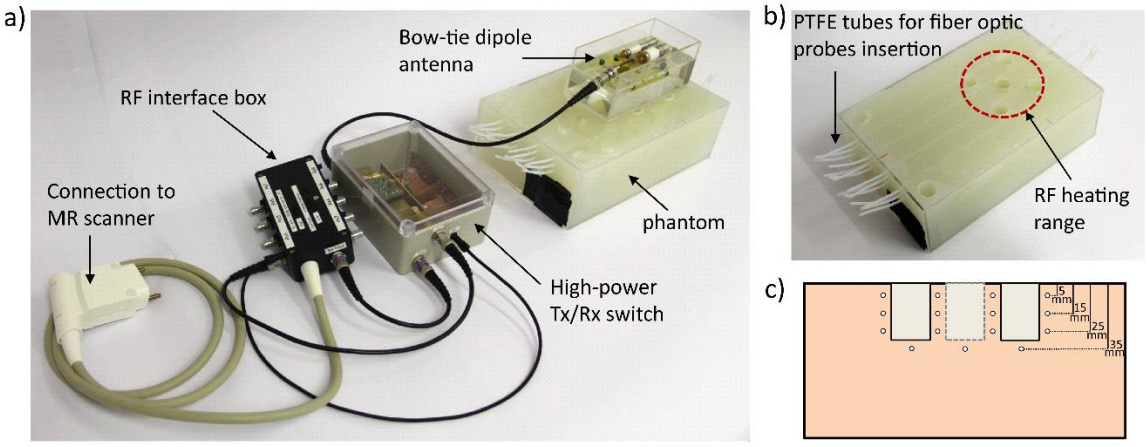

Figure 5 – **a)** RF heating setup. **b)** Agarose phantom with 7 cylindrical sample holders. **c)** Frontal view of the phantom with an indication of the location of the tubes for accommodating fiber optic probes. Image adapted from [1].

RF heating was accomplished using the MR RF power amplifier; 8 kW peak power, 4 ms rectangular pulse, U = 290 V and TR = 40 ms, duty cycle = 10%. This setup afforded a measured average power of 100 W at feeding point of the dipole antenna. The heating paradigm consisted of 3 × 5 min RF heating interleaved with 2D MRTh acquisition. 2D MRTh was conducted using a proton resonance frequency shift method and dual gradient-echo technique (in plane resolution = (1.5 × 1.5) mm^2, slice thickness = 4 mm, matrix size = (192 × 192), number of slices = 3, TR = 61 ms, TE1 = 2.26 ms and TE2 = 11.44 ms, nominal flip angle = 30°, total scan time = 11 s). A fiber optic probe (Omniflex, Neoptix, Quebec, Canada) placed 15 mm below the RF antenna was used as temperature reference.

For comparison, we used a conventional Tx/Rx switch but applied only P_{avg} = 25 W (U = 154 V, 4 ms rectangular pulse, TR = 40 ms, 10% duty cycle) – maximum power established by manufacturer, and performed the same heating paradigm.

2.2. Load release from thermoresponsive carriers

2.2.1. Synthesis and characterization of thermoresponsive nanogels

The themoresponsive nanogels were synthesized using nanoprecipitation methodology with acrylated dendritic polyglycerol (Ac-dPG) as macromolecular cross-linker and temperature-sensitive polymers poly(N-isopropylacrylamide) (PNIPAM) and poly(N-isopropyl methacrylamide) (PNIPMAM) as linear counterpart. The thermoresponsive nanogels were synthesized by my cooperator Dr. Lucila Navarro, Freie Universität Berlin.

The acrylated dendritic polyglycerol (Ac-dPG, 7%) was synthesized with dendritic polyglycerol (dPG) obtained from Nanopartica GmbH, Berlin, Germany with a molecular weight (MW) of 10 kDa and a polydispersive index of 1,3. The dPG was pre-dried in vacuum at 80 °C for 24 h and (7% mol OH groups, 1 eq.) was dissolved in 20 mL of dry dimethylformamide (DMF). The solution was cooled down on ice and triethylene amine (2 eq.) was added to the flask followed by the dropwise addition of acryloyl chloride (1.3 eq.) under argon atmosphere. The

solution was stirred for 4 h and then quenched by adding a small amount of water. Ac-dPG was purified by dialysis using a regenerated cellulose membrane (molecular weight cut-off (MWCO) 1 kDa) in water for 2 days. The product was obtained with a yield of 85-90% and stored at 6-8 °C. The synthesis of Ac-dPG was characterized by ^{1}H-NMR using a 400 MHz NMR spectrometer (Jeol, ECX 400, Tokyo, Japan).

Thermoresponsive nanogels (NGs) were synthesized according to previously reported methodologies [25] with minor modifications. In brief, a total amount of 100 mg of the monomers; 30 mg of Ac-dPG, 42 mg of PNIPAM and 28 mg of PNIPMAM, and 1.8 mg of dodecyl sulfate sodium were dissolved in 4 mL of distilled water. The reaction was purged with argon for 30 minutes and then transferred to an oil bath at 70 °C. After 15 min, 1 mL of a solution of potassium persulfate (3.3 mg/mL) was added to initiate the polymerization. The reaction mixture was stirred for 4 h at 70 °C. The nanogels were purified for 3 days via dialysis (regenerated cellulose, MWCO 50 kDa) in water. The product was lyophilized and rendered a white cotton-like solid in a yield of 80-90%.

The characterization of the structure was performed by ^{1}H-NMR using a 400 MHz NMR spectrometer (Jeol, ECX 400, Tokyo, Japan). The size, the polydispersive index and the volume phase transition temperature (VPTT) of the nanogels were evaluated using dynamic light scattering technique. A Malvern Zetasizer Nano-ZS 90 (Malvern Instrument, Malvern, Worcestershire, UK) equipped with a red He-Ne laser (λ=633 nm, 4.0 mW) was used for the measurement under a scattering angle of 173°. Prior testing, the samples were left to stabilize for 5 min under a certain temperature. The VPTT was determined by measuring the size of the nanogels in a range of 25-55 °C using a heating rate of 1 °C/min. The VPTT is defined as the temperature of the inflection point of the normalized size *vs* temperature curve.

2.2.2. Protein encapsulation in the thermoresponsive nanogels

Bovine serum albumin labeled with fluorescein (BSA-FITC) was used as a model therapeutic for release experiments. To encapsulate the BSA-FITC, the dry nanogel (5 mg) was swollen in 1 mL of a solution of BSA-FITC in phosphate buffer

saline (PBS) (0.5 mg/mL, pH 7.4) for at least 24 h at 4 °C. The solution was purified three times using Vivaspin 300 kDa centrifugal filter (5 mL, 10 min each time, speed = 4800 x g, Vivaspin 6, Sartorius AG, Göttingen, Germany). With this procedure, the nanogels were retained in the concentrate and the non-encapsulated BSA-FITC (MW = 66 kDa) was washed out with the filtrate. The concentration of encapsulated BSA-FITC was determined by fluorescence (excitation wavelength (λ_{ex}) = 490 nm and emission wavelength (λ_{em}) = 525 nm).

2.2.3. Protein Release study in water bath

An initial evaluation of the release profile of the BSA-FITC was evaluated using a water bath as a heat source. The above-mentioned nanogel loaded with BSA-FITC was diluted with buffer (PBS, pH 7.4) to a final concentration of 1 mg/mL of nanogel. Three Vivaspin filters (Vivaspin 500, Sartorius AG, Göttingen, Germany), each with 400 uL of the diluted solution, were placed in the water bath at 20 °C (room temperature), 37 °C and 43 °C. The filters were wrapped with parafilm to avoid contact with water of the water bath. At certain time intervals, the samples were centrifuged (10 min, 4800 x g) and the filtrates were taken for analysis (fluorescence at $\lambda_{ex}/\lambda_{em}$ = 490/525 nm), while the same volume was replaced with fresh buffer. The filters were weighed before and after centrifugation to calculate the volume of buffer to be replaced.

2.2.4. Phantom design for radiofrequency induced heating in an MR scanner

A dedicated phantom was designed to carry out temperature controlled release experiments in a 7.0 T whole-body MR system (Siemens Healthineers, Erlangen, Germany), as depicted in **Figure 6a**.

The phantom comprises a 180 × 280 × 90 mm^3 rectangular box filled with agarose gel (20 g/L) dopped with NaCl (5 g/L) and $CuSO_4$ (0.7 g/L), yielding a conductivity (σ) of 1.03 S/m and a relative permittivity (ε_r) of 71.9 at 297.2 MHz (working frequency of the MR scanner). Seven cylinder containers with inner diameter = 22 mm and height = 30 mm were inserted into the phantom as sample holders (**Figure 6b**): five were placed in the hotspot area produced by bow-tie dipole antenna (for heated sample), and the other two were placed where the antenna

would not produce temperature rise (for control sample). Polytetrafluoroethylene (PTFE) tubes with inner diameter = 1 mm were inserted along the long axis of the phantom at depth of 5 mm, 15 mm, 25 mm and 35 mm (**Figure 6c**) to accommodate fiber optic probes that serve as temperature reference for MR thermometry (MRTh). The phantom could be placed in a water box connected to a water bath to modify the background temperature.

Electromagnetic field simulation using the finite-difference time-domain method and temperature simulations solving Pennes bioheat equation (Sim4life, ZMT AG, Zurich, Switzerland) were performed to study the heat distribution induced by radiofrequency energy in the phantom. The simulation setup is depicted in **Figure 6d**; the phantom was placed inside a water box (250 × 360 × 120) mm^3, with background temperature set as 37 °C, and a bow-tie dipole antenna was placed on top, centered on the heated sample. The basic mesh resolution of (5 × 5 × 5) mm^3 was locally refined to (0.5 × 0.5 × 0.5) mm^3 in order to secure all electrical connections, resulting in a total mesh of 10 million cells. The electromagnetic field simulations were performed at 297.2 MHz, the working frequency of the MR scanner.

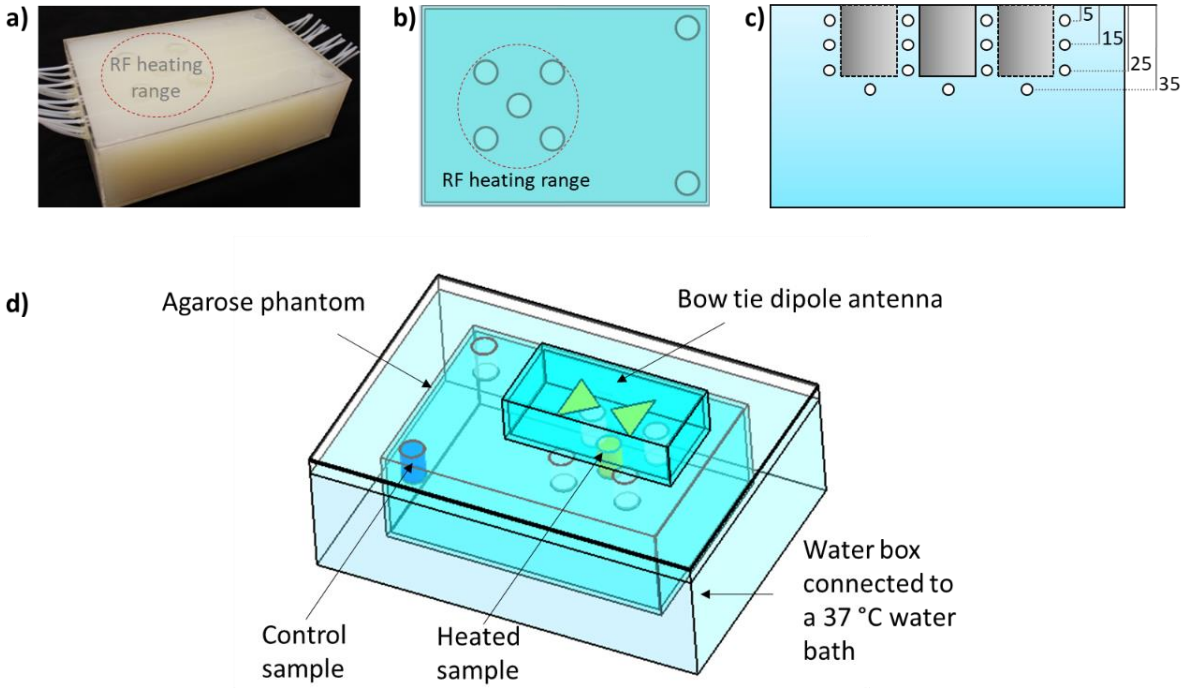

Figure 6 – **a)** Agarose phantom with sample holders, five in the center of RF heating range and two outside of this range. **b)** Schematics of the phantom, top view. **c)**

Schematics of the phantom, frontal view with the positioning of the PTFE tubes for the insertion of fiber optic temperature sensors. The PTFE tubes were placed at each side of the sample holders (note, the holders are not all in the same plane) at a depth of 5, 15 and 25 mm and at bottom of the holders at a depth of 35 mm). **d)** Setup for the electromagnetic field and temperature simulations. The phantom was placed inside a water box with background temperature of 37 °C, and a bow-tie dipole antenna was placed on top, centered in the heated sample.

2.2.5. Experimental setup for radiofrequency induced heating in an MR scanner

The radiofrequency (RF) heating induced release experiment was carried out in a whole body 7.0 T MR system using one bow-tie dipole antenna. The experimental setup (**Figure 7**) was comprised by i) three Vivaspin filters with 400 uL of the nanogel – (BSA-FITC) solution, ii) the agarose gel phantom, iii) the water box connected to a water bath to keep the background temperature at 37 °C, iv) a bow-tie dipole antenna for imaging and RF energy delivering, v) a customized high power transmit/receive (Tx/Rx) switch [1] to support high-power RF pulses and vi) fiber optic temperature sensors (Omniflex, Neoptix, Quebec, Canada) used as external temperature reference.

The phantom was placed in the water box and preheated overnight to 37 °C. In the next day, one vivaspin filter was placed in the middle sample holder of the hotspot area of the phantom, a second filter was placed in the control sample holder beyond the hotspot and a third filter was kept outside the MRI scanner room in the lab at room temperature (20 °C). All the sample holders were filled with 0.1 M NaCl solution (σ = 1.05 S/m, ε = 80.4) to avoid susceptibility artifacts. Four fiber optic temperature sensors were placed in the middle sample holder (heated sample), in the control sample holder, inside the phantom at depth of 15 mm next to the middle sample holder, and inside the phantom at depth of 25 mm next to the middle sample holder. Then, the bow-tie dipole antenna would be placed on the lid of the water box, centered on the middle sample holder of the phantom. Next, the bow-tie dipole antenna would be tuned and matched to the B_0 field frequency of the MR scanner (f = 297.2 MHz), then connected to the customized high power Tx/Rx switch and the switch to the scanner.

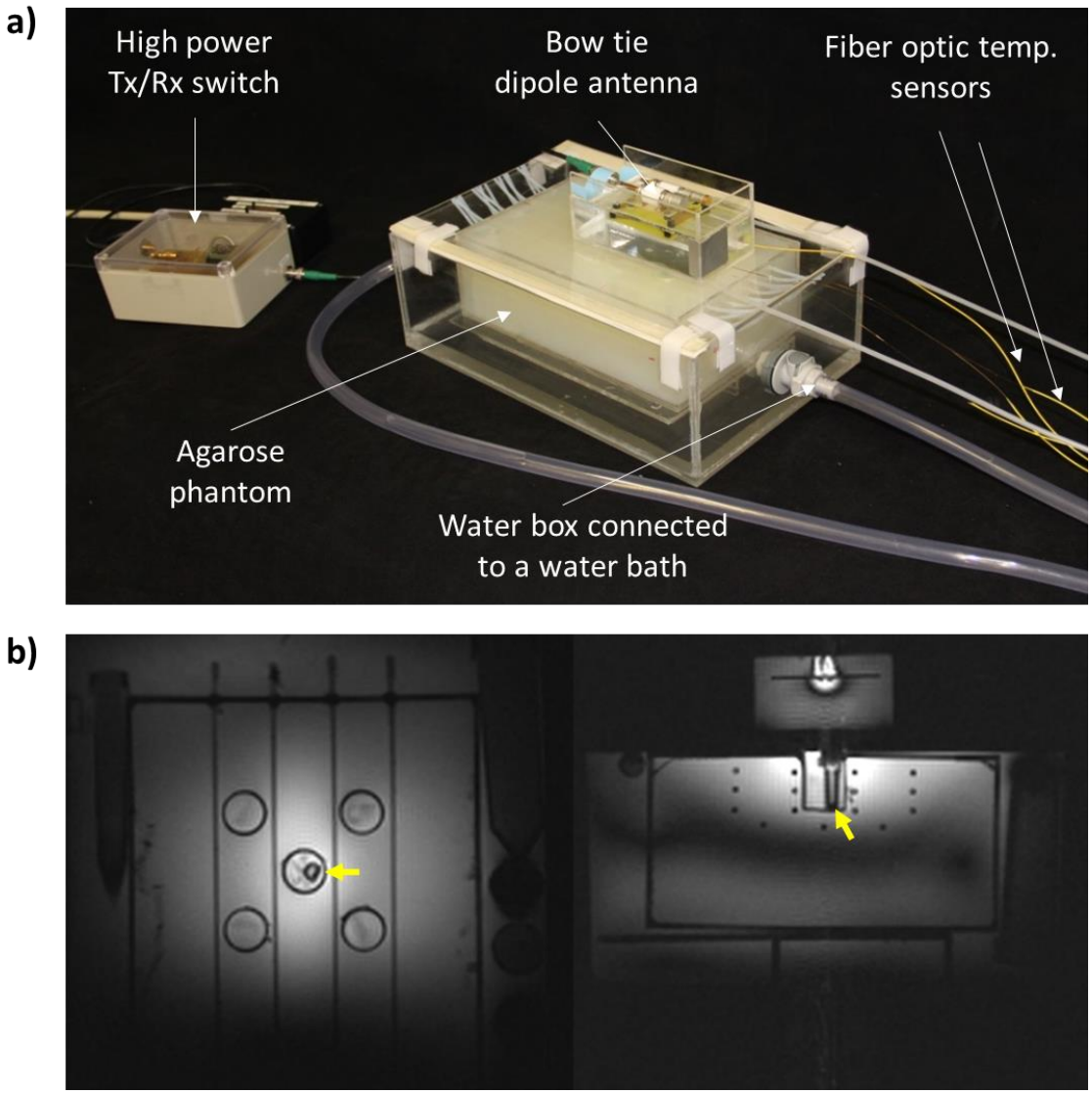

Figure 7 – **a)** Photograph of the RF heating setup for the MR scanner; the agarose gel phantom for holding the Vivaspin filter with the BSA-FITC loaded nanogels, the water box connected to a water bath for background temperature modification (in this case 37 °C), a bow-tie dipole antenna for imaging and RF heating, a customized high-power Tx/Rx switch and fiber optic temperature sensors as temperature reference for MR thermometry. **b)** MR images of the phantom. The vivaspin tube with the nanogel sample in the middle sample holder (heated sample) is indicated by the yellow arrows. Left: axial view at a depth of 15 mm (at the level of the second row of the PTFE tubes). Right: axial view at the center of the middle sample holder.

2.2.6. Radiofrequency induced heating paradigm and protein release study

The heating paradigm consisted of sending RF pulses with average power (P_{avg}) = 100 W at antenna feeding point for 15 minutes, interleaved every 5 minutes with 2D MR thermometry (MRTh) measurements.

The RF power is provided by the 7.0 Tesla MR system amplifiers (8 kW peak power) with a rectangular pulse of 4 ms (U = 280 V) and TR of 40 ms, resulting in a duty cycle of 10%. The hardware losses between the transmitter and the feeding point of the bow-tie dipole antenna were 2.12 dB.

MRTh was conducted using a proton resonance frequency shift method [26] and dual gradient-echo technique [27,28] (FOV = (290 × 290) mm^2, TR = 102ms, TE1 = 2.26 ms and TE2 = 11.44 ms, spatial resolution = (1.5 × 1.5 × 4) mm^3, nominal flip angle = 30°). Fiber optic temperature sensors were used as external reference for the MRTh temperature maps.

After reaching 43°C in the middle sample holder, the temperature was maintained with subsequent RF pulses for 1 to 2 minutes. At certain time intervals, Vivaspin filters were taken out, centrifuged (10 min, 4800 x g) and the filtrates were taken for analysis (fluorescence at $\lambda_{ex}/\lambda_{em}$ = 490/525 nm). Then, the fresh buffer was replaced and Vivaspin filters were placed again in the phantom. The filters were weighed before and after centrifugation to calculate the volume of buffer to be replaced.

3. Results

3.1. High-power Tx/Rx switch

3.1.1. Tx/Rx switch performance

The high-power Tx/Rx switch provided isolation of -29 dB between transmission port and receive port during the transmission mode and -39.1 dB during receive mode. The insertion loss was -0.3 dB between the Tx port and the antenna in the transmission mode and -0.3 dB between the antenna and the Rx port in the receive mode.

After operating at an average power P_{avg} = 100 W for 30 min, the maximum temperature in the circuit of high-power Tx/Rx switch was 59.7 °C, in an inductor of receive compartment (**Figure 8a,c**). In comparison, the conventional imaging Tx/Rx switch circuit reached 97.5 °C in a pin diode after operating at 100 W for 2 min (**Figure 8b,d**).

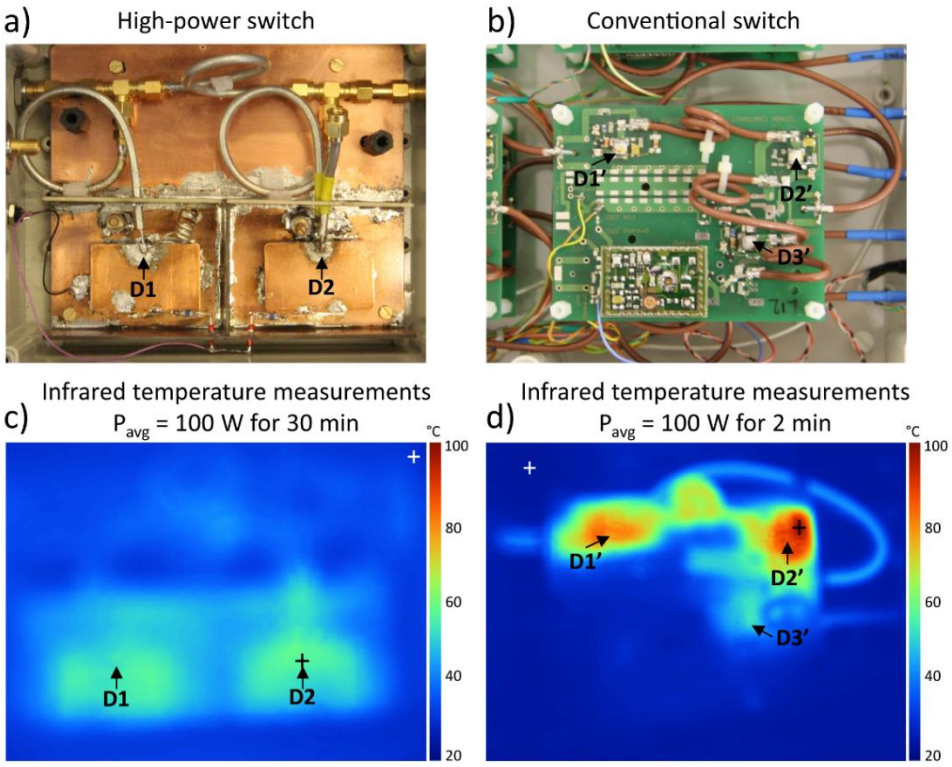

Figure 8 – **a)** high power Tx/Rx switch and **b)** conventional Tx/Rx switch driving 100 W. **c)** Temperature in the circuit of high power switch after 30 min; background temperature (white +) = 24.9 °C, highest temperature (black +) = 59.7 °C. **d)** Temperature in

conventional switch after 2 min; background temperature (white +) = 23.7 °C, highest temperature (black +) = 97.5 °C. Image adapted from [1].

3.1.2. MR imaging test

The high spatial resolution MR images (**Figure 9**) acquired with the high power Tx/Rx switch and a conventional Tx/Rx switch yielded similar image quality. On both images, one could appreciate many small structures such as carpal bones, ulnar disc, radio-carpal and ulnar-carpal joints and cartilage. The signal to noise ratio was 30.3 for high power Tx/Rx switch and 25.4 for conventional switch.

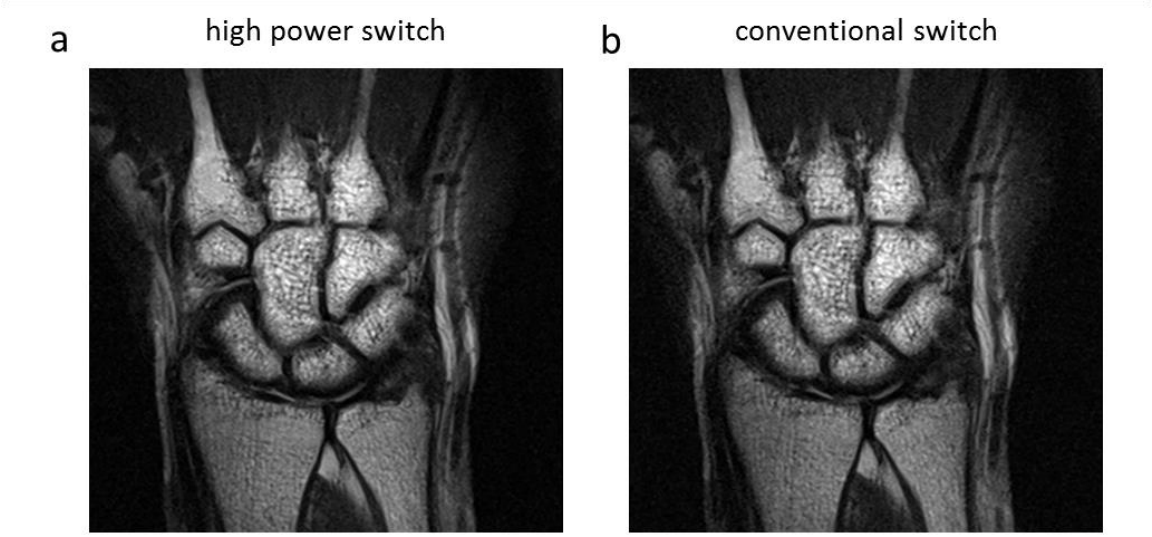

Figure 9 – Wrist MRI performed with a) high power Tx/Rx switch and b) conventional switch. Image adapted from [1].

3.1.3. RF induced heating and MR thermometry

In the RF heating experiments, the temperature increase in the phantom is greater when high power Tx/Rx switch was used; as higher power (100 W vs 25 W) could be delivered.

In the high power Tx/Rx switch setup, after 5, 10 and 15 min of RF heating with P_{avg} = 100 W, the temperature increase in the phantom at the depth of 15 mm (**Figure 10a**) was 5.9 ± 0.26, 13.6 ± 0.60 and 18.5 ± 0.40 °C, obtained from MRTh maps. The fiber optic probe positioned at the same location registered 6.7, 12.4

and 17.5 °C (**Figure 10b**). Temperature measured with MRTh and fiber optic probe had a deviation of 0.8-1.2 °C.

In comparison, the temperature increase in the same location while using a conventional Tx/Rx switch with P_{avg} = 25 W (maximum P_{avg} allowed by manufacturer) was 2.3 ± 0.38, 4.3 ± 0.45 and 5.3 ± 0.37 °C obtained from MRTh maps and 1.7, 3.5 and 4.7 °C registered by the fiber optic probe (**Figure 10b**). Temperature measured with MRTh and fiber optic probe had a deviation of 0.6-0.8 °C.

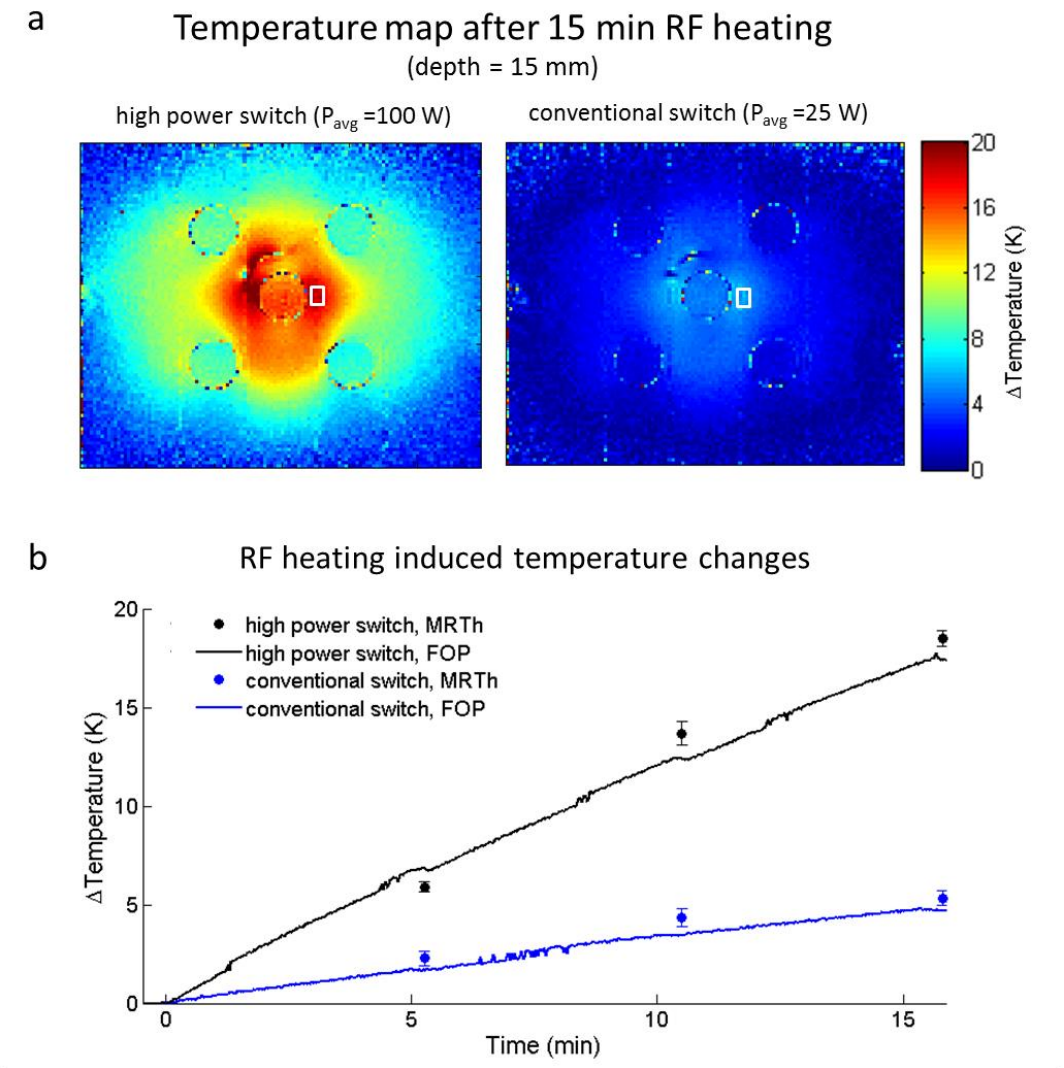

Figure 10 – RF heating with high-power Tx/Rx switch, P_{avg} = 100 W vs conventional Tx/Rx switch, P_{avg} = 25 W. **a)** temperature maps calculated from MR thermometry (MRTh) using PRF method. **b)** temperature readings from MRTh maps and fiber optic probes (FOP). Image adapted from [1].

3.2. Load release from thermoresponsive carriers

3.2.1. Thermoresponsive nanogel characterization

The synthesis of the Ac-dPG was confirmed by the chemical shifts in the ^{1}H-NMR spectrum (**Figure 11a**): 3.1-4.5 ppm (multiplet, 5 H, polyglycerol protons), 5.98-6.10 ppm (multiplet, 1 H, vinyl group), 6.15-6.30 ppm (multiplet, 1 H, vinyl group), 6.40-6.53 ppm (multiplet, 1 H, viniyl group).

By dynamic light scattering, the size of the nanogels was determined to be 105 nm with a polydispersive index of 0.110. The structure of the nanogels was confirmed by the chemical shifts in the ^{1}H-NMR spectrum (**Figure 11b**): 1.16 ppm (singlet, 6 H, isopropyl groups of PNIPAM and PNIPMAM), 1.57-2.17 ppm (multiplet, 3 H of polymer backbone of PNIPAM plus 2 H of polymer backbone of PNIPMAM), 3.37-4.10 ppm (multiplet, 7 H, polyglycerol scaffold protons plus 1 H of PNIPAM plus 1 H of PNIPMAM).

The volume phase transition temperature (VPTT) defined as the temperature of the inflection point of the size *vs* temperature curve (**Figure 11c**) is found to be 38 °C.

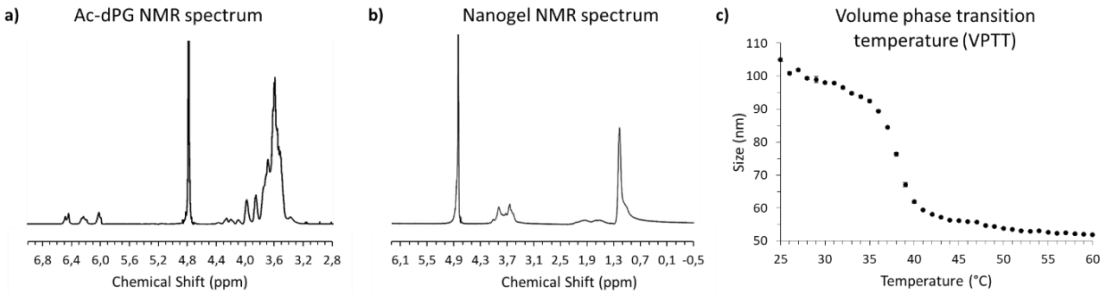

Figure 11 – **a)** The synthesis of acrylated dendritic polyglycerol (Ac-dPG) was confirmed by the chemical shifts in the ^{1}H-NMR spectrum: 3.1-4.5 ppm (multiplet, 5 H, polyglycerol protons), 5.98-6.10 ppm (multiplet, 1 H, vinyl group), 6.15-6.30 ppm (multiplet, 1 H, vinyl group), 6.40-6.53 ppm (multiplet, 1 H, viniyl group). D2O was used as solvent (4.8 ppm). **b)** The structure of the nanogels was confirmed by the chemical shifts in the ^{1}H-NMR spectrum: 1.16 ppm (singlet, 6 H, isopropyl groups of PNIPAM and PNIPMAM), 1.57-2.17 ppm (multiplet, 3 H of polymer backbone of PNIPAM plus 2 H of polymer backbone of PNIPMAM), 3.37-4.10 ppm (multiplet, 7 H, polyglycerol scaffold protons plus 1 H of PNIPAM plus 1 H of PNIPMAM). D2O was used as solvent (4.8 ppm). **c)** Nanogel size vs temperature curve. The volume phase transition temperature (VPTT) defined as the temperature of the inflection point of this curve is found to be 38 °C. Data collected by Dr. Lucila Navarro, Freie Universität Berlin.

3.2.2. Protein release from nanogel: in water bath

The release of BSA-FITC from the nanogels using water bath as a heat source is shown in the graph of **Figure 12**.

At room temperature of 20 °C (18 °C lower than VPTT = 38 °C), the release of the BSA-FITC from the nanogels was 12.5% after 6 hours and 14.1% after 19 hours.

At 37 °C (1 °C less than VPTT), the release of the BSA-FITC from the nanogels was 19.5% after 6 hours and 27.6% after 19 hours.

At 43 °C (5 °C higher than the VPTT) the release of the BSA-FITC from the nanogels was 32.8% after 6h and 43.6% after 19 hours.

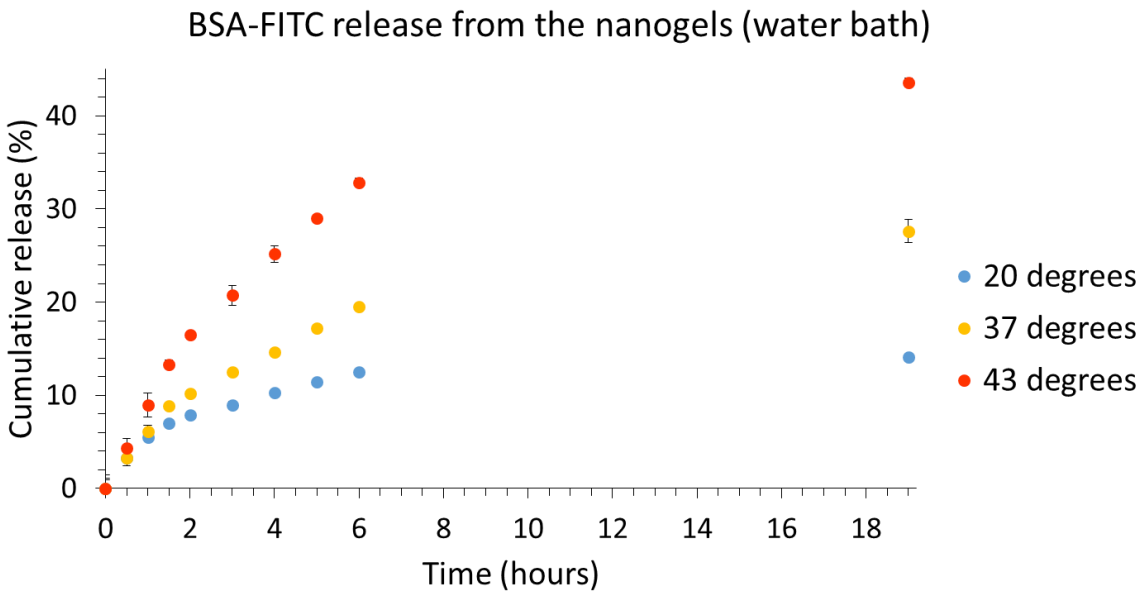

Figure 12 – Bovine saline albumin labelled with fluorescein (BSA-FITC) release from the nanogels using water bath as heat source. After 6 hours, 12.5%, 19.5% and 32.8% of the BSA-FITC were released from the nanogels at 20 °C, 37 °C and 43 °C, respectively. After 19 hours, 14.1%, 27.6% and 43.6% of the BSA-FITC were released from the nanogels at 20 °C, 37 °C and 43 °C, respectively.

3.2.3. Temperature simulations of the phantom

The temperature maps (**Figure 13**) obtained from the electromagnetic and thermal simulations of the phantom using a background temperature of 37 °C yielded T = 43 °C (t = 11 min, P_{avg} = 100 W) for the middle sample holder. The temperature obtained for the controlled sample holder remained constant at T=37 °C.

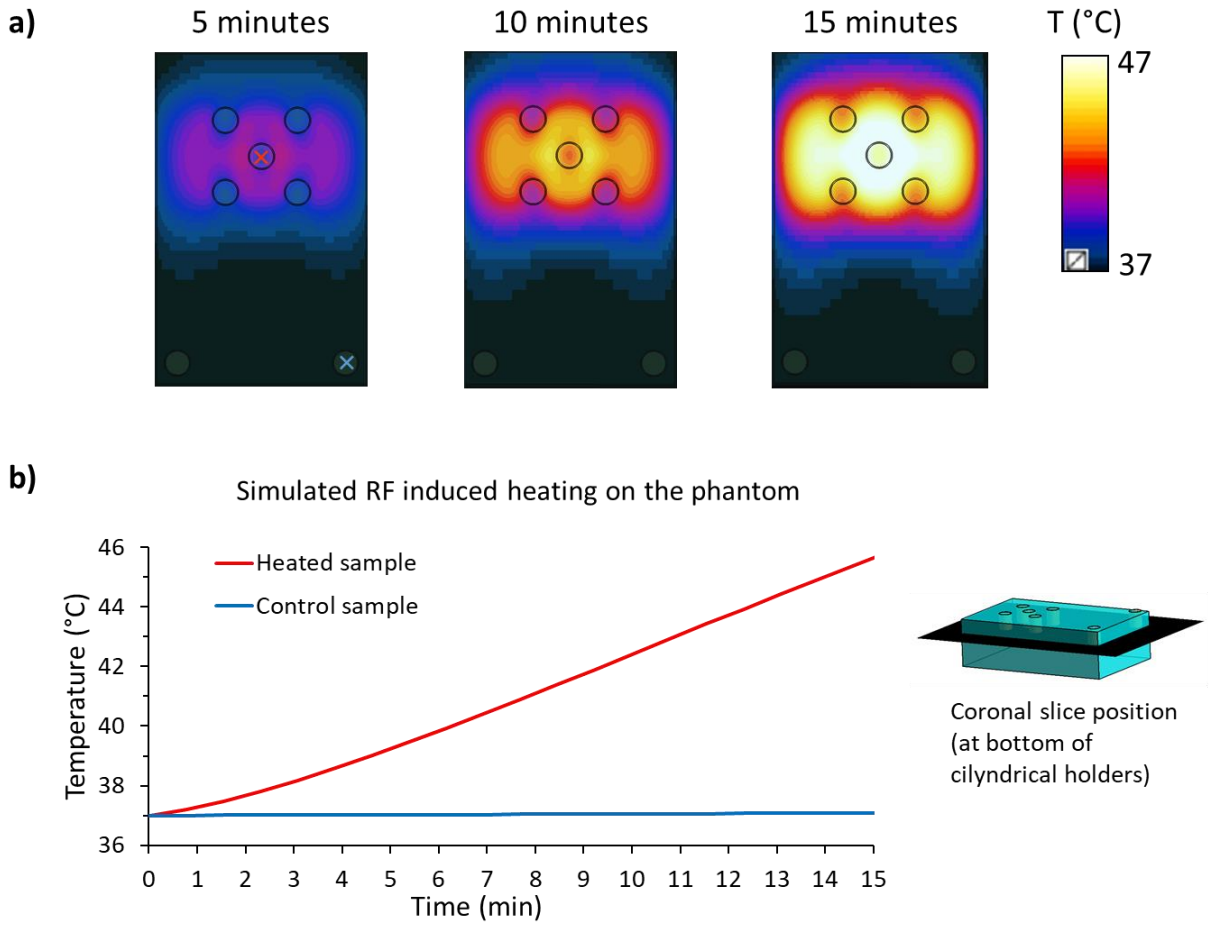

Figure 13 – Simulated radiofrequency induced heating in the phantom with P_{avg} = 100 W for 15 minutes. **a)** Simulated temperature distribution in the phantom (depth = 25 mm, coronal plane) at 5, 10 and 15 minutes. **b)** Time dependent temperature evolution in the heated sample (red cross) compared to the control sample (blue cross). The schematic of the phantom on the right hand side shows the coronal plan where the temperature distribution maps were taken. The data shows that the RF heating is constrained to the central sample, while the control sample temperature profile is unaffected.

3.2.4. RF heating of the phantom

The temperature changes in the phantom during RF heating were accessed with readings from fiber optic temperature sensors and MR thermometry (MRTh) and it is shown in **Figure 14**.

The fiber optic temperature sensor readings from the controlled sample holder maintained consistently at 37 °C. In the heated sample, the reading was 38.8 °C after the first 5 minutes of RF heating, 40.9 °C after the second 5 minutes RF heating and 43.4 after the third 5 minutes of RF heating.

The reading from the fiber optic temperature sensor inside the phantom at 25 mm was 38.8 °C after the first 5 min RF heating session, while the temperature map obtained with MR thermometry at that moment showed 38.6 °C. After the second 5 min RF heating, the fiber optic temperature sensor registered 40.47 °C, and the MRTh 40.0 °C. Finally, after the last 5 minutes of RF heating, the fiber optic temperature sensor marked 42.5 °C, and the MRTh 41.7 °C.

3.2.5. Protein release from nanogel: Thermal MR

The release of BSA-FITC from the nanogels using RF energy as heat source (thermal MR) is shown in graph of the **Figure 15**.

At room temperature of 20 °C (18 °C lower than VPTT = 38 °C), the release of the BSA-FITC from the nanogels was 12.9% after 6 hours.

At 37 °C (1 °C less than VPTT), the release of the BSA-FITC from the nanogels was 19.6% after 6 hours.

At 43 °C (5 °C higher than the VPTT), the release of the BSA-FITC from the nanogels was 29.3% after 6 hours.

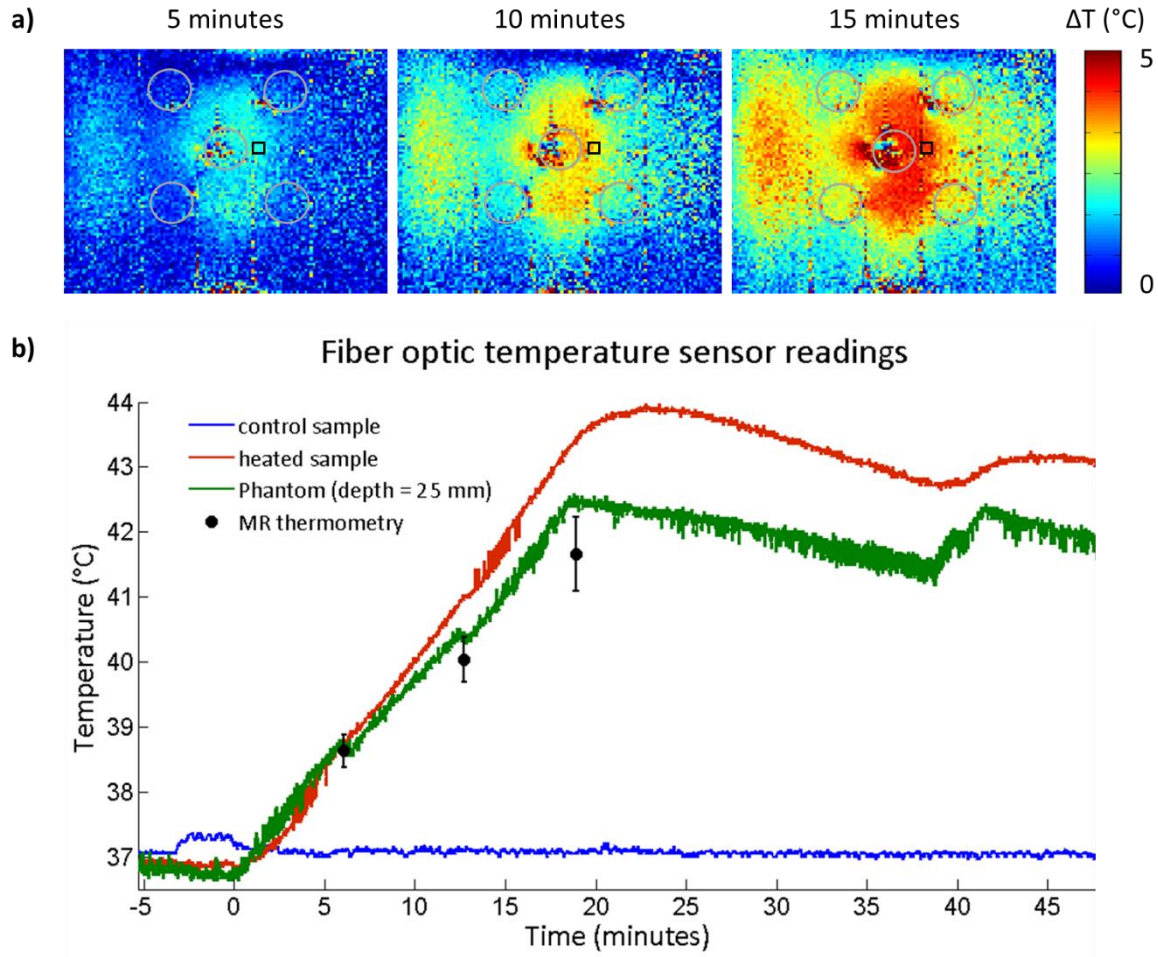

Figure 14 – **a)** Temperature distribution maps in the phantom at depth = 25 mm obtained with MR thermometry. To guide the eye, the grey circles were inserted to mark the sample holders and the black rectangle marked the position of the fiber optic temperature sensor. **b)** The temperature along time from the fiber optic temperature sensor readings in the controlled sample holder (blue), in the heated sample holder (red) and inside phantom next to the heated sample (black rectangle in a), and temperature obtained by MR thermometry at position of black rectangle.

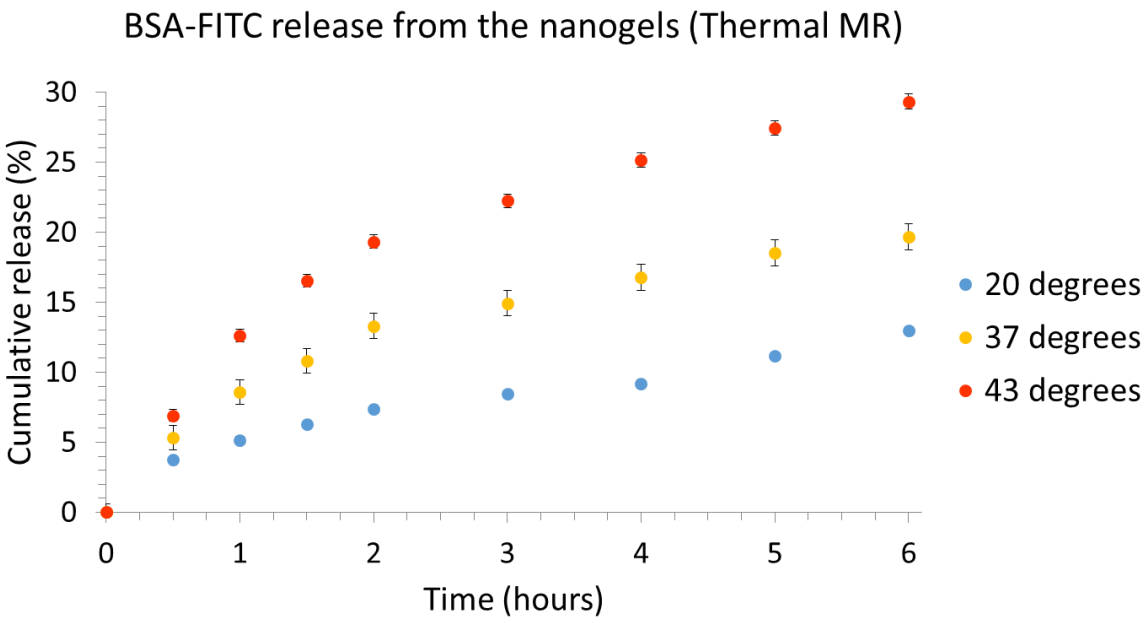

Figure 15 – Bovine serum albumin labelled with fluorescein (BSA-FITC) released from the nanogels using RF heating from thermal MR. After 6 hours, 12.9%, 19.6% and 29.3% of the BSA-FITC were released from the nanogels at 20 °C, 37 °C and 43 °C, respectively.

4. Discussion and Conclusion

In the first part of this work, the constructed high power Tx/Rx switch for thermal MR applications provided high isolation and low insertion loss. When benchmarked against a conventional Tx/Rx switch, it proved to be capable of handling a high average power, necessary for RF heating (100 W) without causing overheating in the circuit. This shows that the design of high power Tx/Rx switch was effectively blocking the RF waves from the lossy pin diodes preventing energy loss that was translated into increased temperature in the conventional Tx/Rx switch. Overheating in the circuit is unsafe as it can burn up electronic components or cause melting of solder inducing open or short circuits that compromise the overall performance of the circuit.

When tested for MR imaging, the high power Tx/Rx switch supported high resolution imaging of the wrist. The many small and clinically relevant structures such as carpal bones, discs, joints, and cartilage are well depicted in the images. Compared to a conventional Tx/Rx switch, the high power Tx/Rx switch displayed similar image quality.

The RF heating experiments showed the limitation of conventional switch and thus the need for an alternative circuit design that could handle higher power demands. The high power switch design could support RF heating with average power of 100 W. Although only one bow tie antenna was used, after 5 min it could induce ~6 °C of temperature increase at the depth of 15 mm of the phantom. In a biological system, an increase of 6 °C will put it under hyperthermia conditions.

Upon the positive results obtained by hardware development, in the second part of this work, the thermal intervention potential of the setup was exploited to demonstrate the feasibility of the temperature induced release of a protein from a thermoresponsive nanogel in a 7.0 T MR system.

The reference release profile obtained with a water bath setup used for temperature intervention is in accordance with the release kinetics deduced from the thermal MR setup. This finding supports the feasibility of thermal MR for temperature controlled release of a load from thermoresponsive nanocarriers.

In this study, a single bow-tie dipole antenna has been used for imaging, temperature intervention, and temperature monitoring. This approach constrained the heating rate to $\Delta T = 0.3$ °C per minute for a peak power of P = 100 W and a duty cycle of 10%. To enhance the heating rate, an array of RF antenna can be exploited [6,29]. This approach would afford shaping and steering of the temperature hotspot and would support parallel MR imaging to reduce acquisition times needed for temperature monitoring of larger volumes [30,31].

In this work, a fluorescence labelled protein was loaded to thermoresponsive nanogels and the release characteristics were studied with fluorescence spectroscopy upon conventional water bath heating or after Thermal MR intervention. Swift translation of Thermal MR triggered release of a load from a nanocarrier remains conceptually appealing and an ambitious undertaking en route to clinical feasibility studies of thermal therapeutics. For the assessment of the efficacy of thermal interventions, it is of paramount importance to examine the release rate and kinetics in vivo. Here, thermoresponsive nanocarriers loaded with MR sensitive fluorine probes could provide ideal means to monitor release kinetics and bioavailability [32] of the MR visible load in vivo, which would be a major leap forward to temperature induced drug delivery. While the current work used a thermoresponsive nanogel as a carrier, the Thermal MR triggered release of payloads from other thermoresponsive carriers is to be expected to be also feasible. Further smart carriers that, in addition to temperature, also respond to internal variation in the microenviroment of certain diseases [14,19] (pH variations, hormone concentrations, redox gradient, etc.) are also interesting study candidates.

MRI is a vital clinical tool for diagnosis and for guiding therapy. MRI has been described as one of the most important medical innovations [33,34]. Current clinical MR approaches offer no integrated means for diagnosis and thermal intervention (thermo-theranostics), inherent to the RF fields applied. Simultaneously accommodating thermal diagnostics, intervention and response control is conceptually intriguing for the pursuit personalized therapeutic approaches for better patient care and for the study of the role of temperature in biology and disease. In conclusion, the Thermal MR approach adds a thermal

intervention dimension to an MR imaging device and provides an ideal testbed for the study of temperature induced release of drugs, MR probes and other agents from thermoresponsive smart carriers.

5. References

[1] Y. Ji, W. Hoffmann, M. Pham, A.E. Dunn, H. Han, C. Özerdem, H. Waiczies, M. Rohloff, B. Endemann, C. Boyer, M. Lim, T. Niendorf, L. Winter, High peak and high average radiofrequency power transmit/receive switch for thermal magnetic resonance, Magn. Reson. Med. 80 (2018) 2246–2255.

[2] N. van den Tempel, M.R. Horsman, R. Kanaar, Improving efficacy of hyperthermia in oncology by exploiting biological mechanisms, Int. J. Hyperth. 32 (2016) 446–454.

[3] E. Martin, D. Jeanmonod, A. Morel, E. Zadicario, B. Werner, High-intensity focused ultrasound for noninvasive functional neurosurgery, Ann. Neurol. Off. J. Am. Neurol. Assoc. Child Neurol. Soc. 66 (2009) 858–861.

[4] P. Wust, B. Hildebrandt, G. Sreenivasa, B. Rau, J. Gellermann, H. Riess, R. Felix, P.M. Schlag, Hyperthermia in combined treatment of cancer, Lancet Oncol. 3 (2002) 487–497.

[5] M.A. Ward, T.K. Georgiou, Thermoresponsive polymers for biomedical applications, Polymers (Basel). 3 (2011) 1215–1242.

[6] L. Winter, C. Özerdem, W. Hoffmann, D. Santoro, A. Müller, H. Waiczies, R. Seemann, A. Graessl, P. Wust, T. Niendorf, Design and evaluation of a hybrid radiofrequency applicator for magnetic resonance imaging and RF induced hyperthermia: electromagnetic field simulations up to 14.0 Tesla and proof-of-concept at 7.0 Tesla, PLoS One. 8 (2013) e61661.

[7] IEC 60601-2-33 ed3.0 - Medical electrical equipment - Part 2-33: Particular requirements for the basic safety and essential performance of magnetic resonance equipment for medical diagnosis, (2010). http://webstore.iec.ch/webstore/webstore.nsf/Artnum_PK/43851.

[8] L. Winter, C. Oezerdem, W. Hoffmann, T. van de Lindt, J. Periquito, Y. Ji, P. Ghadjar, V. Budach, P. Wust, T. Niendorf, Thermal magnetic resonance: physics considerations and electromagnetic field simulations up to 23.5 Tesla (1GHz), Radiat. Oncol. 10 (2015) 201.

[9] R. Langer, Drug delivery and targeting, NATURE-LONDON-. (1998) 5–10.

[10] T.M. Allen, P.R. Cullis, Drug delivery systems: entering the mainstream, Science (80-.). 303 (2004) 1818–1822.

[11] K. Park, Controlled drug delivery systems: past forward and future back, J. Control. Release. 190 (2014) 3–8.

[12] N. Kamaly, B. Yameen, J. Wu, O.C. Farokhzad, Degradable controlled-release polymers and polymeric nanoparticles: mechanisms of controlling drug release, Chem. Rev. 116 (2016) 2602–2663.

[13] J. Panyam, V. Labhasetwar, Biodegradable nanoparticles for drug and gene delivery to cells and tissue, Adv. Drug Deliv. Rev. 55 (2003) 329–347.

[14] J.A. Barreto, W. O'Malley, M. Kubeil, B. Graham, H. Stephan, L. Spiccia, Nanomaterials: applications in cancer imaging and therapy, Adv. Mater. 23 (2011) H18–H40.

[15] S. Langereis, J. Keupp, J.L.J. van Velthoven, I.H.C. de Roos, D. Burdinski, J.A. Pikkemaat, H. Grüll, A temperature-sensitive liposomal 1H CEST and 19F contrast agent for MR image-guided drug delivery, J. Am. Chem. Soc. 131 (2009) 1380–1381.

[16] S. Mura, J. Nicolas, P. Couvreur, Stimuli-responsive nanocarriers for drug delivery, Nat. Mater. 12 (2013) 991.

[17] S. Ganta, H. Devalapally, A. Shahiwala, M. Amiji, A review of stimuli-responsive nanocarriers for drug and gene delivery, J. Control. Release. 126 (2008) 187–204.

[18] M. Calderón, M.A. Quadir, M. Strumia, R. Haag, Functional dendritic polymer architectures as stimuli-responsive nanocarriers, Biochimie. 92 (2010) 1242–1251.

[19] D. Liu, F. Yang, F. Xiong, N. Gu, The smart drug delivery system and its clinical potential, Theranostics. 6 (2016) 1306.

[20] A.E. Dunn, D.J. Dunn, A. Macmillan, R. Whan, T. Stait-Gardner, W.S. Price, M. Lim, C. Boyer, Spatial and temporal control of drug release through pH and alternating magnetic field induced breakage of Schiff base bonds, Polym. Chem. 5 (2014) 3311–3315.

[21] P.C. Lyon, L.F. Griffiths, J. Lee, D. Chung, R. Carlisle, F. Wu, M.R. Middleton, F. V Gleeson, C.C. Coussios, Clinical trial protocol for TARDOX: a phase I study to investigate the feasibility of targeted release of lyso-thermosensitive liposomal doxorubicin (ThermoDox®) using focused ultrasound in patients with liver tumours, J. Ther. Ultrasound. 5 (2017) 28.

[22] Y.-C. Chen, L.-C. Liao, P.-L. Lu, C.-L. Lo, H.-C. Tsai, C.-Y. Huang, K.-C. Wei, T.-C. Yen, G.-H. Hsiue, The accumulation of dual pH and temperature responsive micelles in tumors, Biomaterials. 33 (2012) 4576–4588.

[23] G.A. Koning, A.M.M. Eggermont, L.H. Lindner, T.L.M. ten Hagen, Hyperthermia and thermosensitive liposomes for improved delivery of chemotherapeutic drugs to solid tumors, Pharm. Res. 27 (2010) 1750–1754.

[24] L.E. Theune, R. Charbaji, M. Kar, S. Wedepohl, S. Hedtrich, M. Calderón, Critical parameters for the controlled synthesis of nanogels suitable for temperature-triggered protein delivery, Mater. Sci. Eng. C. 100 (2019) 141–151.

[25] J.C. Cuggino, M.C. Strumia, P. Welker, K. Licha, D. Steinhilber, R.-C.

Mutihac, M. Calderón, Thermosensitive nanogels based on dendritic polyglycerol and N-isopropylacrylamide for biomedical applications, Soft Matter. 7 (2011) 11259–11266.

[26] Y. Ishihara, A. Calderon, H. Watanabe, K. Okamoto, Y. Suzuki, K. Kuroda, Y. Suzuki, A precise and fast temperature mapping using water proton chemical shift, Magn. Reson. Med. 34 (1995) 814–823.

[27] V. Rieke, K. Butts Pauly, MR thermometry, J. Magn. Reson. Imaging An Off. J. Int. Soc. Magn. Reson. Med. 27 (2008) 376–390.

[28] U. Wonneberger, B. Schnackenburg, W. Wlodarczyk, T. Walter, F. Streitparth, J. Rump, U.K.M. Teichgräber, Intradiscal temperature monitoring using double gradient-echo pulse sequences at 1.0 T, J. Magn. Reson. Imaging. 31 (2010) 1499–1503.

[29] E. Oberacker, A. Kuehne, J. Nadobny, S. Zschaeck, M. Weihrauch, H. Waiczies, P. Ghadjar, P. Wust, T. Niendorf, L. Winter, Radiofrequency applicator concepts for simultaneous MR imaging and hyperthermia treatment of glioblastoma multiforme, Curr. Dir. Biomed. Eng. 3 (n.d.) 473–477.

[30] T. Niendorf, D.K. Sodickson, Parallel imaging in cardiovascular MRI: methods and applications, NMR Biomed. An Int. J. Devoted to Dev. Appl. Magn. Reson. Vivo. 19 (2006) 325–341.

[31] D.K. Sodickson, C.J. Hardy, Y. Zhu, R.O. Giaquinto, P. Gross, G. Kenwood, T. Niendorf, H. Lejay, C.A. McKenzie, M.A. Ohliger, Rapid Volumetric MRI Using Parallel Imaging With Order-of-Magnitude Accelerations and a 32-Element RF Coil Array: Feasibility and implications1, Acad. Radiol. 12 (2005) 626–635.

[32] Y. Ji, H. Waiczies, L. Winter, P. Neumanova, D. Hofmann, J. Rieger, R. Mekle, S. Waiczies, T. Niendorf, Eight-channel transceiver RF coil array tailored for 1H/19F MR of the human knee and fluorinated drugs at 7.0 T, NMR Biomed. 28 (2015) 726–737.

[33] V.R. Fuchs, H.C. Sox Jr, Physicians' views of the relative importance of thirty medical innovations, Health Aff. 20 (2001) 30–42.

[34] K. Vyas, 10 Medical Inventions of All Time That Changed the World, (n.d.). https://interestingengineering.com/10-medical-inventions-of-all-time-that-changed-the-world (accessed August 29, 2019).

Statutory Declaration

“I, Yiyi Ji, by personally signing this document in lieu of an oath, hereby affirm that I prepared the submitted dissertation on the topic "Radiofrequency induced heating for controlled release of a load from thermoresponsive carriers: a 7.0 Tesla Thermal Magnetic Resonance Study" / "Radiofrequenz induzierte und kontrollierte Freisetzung einer Ladung aus thermoreaktiven Trägern: Thermale Magnetresonanz bei 7.0 Tesla", independently and without the support of third parties, and that I used no other sources and aids than those stated.
All parts which are based on the publications or presentations of other authors, either in letter or in spirit, are specified as such in accordance with the citing guidelines. The sections on methodology (in particular regarding experimental work, data collection and analysis) and results (in particular regarding figures, charts and tables) are exclusively my responsibility.

My contributions to any publications to this dissertation correspond to those stated in the below joint declaration made together with the first supervisor. All publications created within the scope of the dissertation comply with the guidelines of the ICMJE (International Committee of Medical Journal Editors; www.icmje.org) on authorship. In addition, I declare that I am aware of the regulations of Charité – Universitätsmedizin Berlin on ensuring good scientific practice and that I commit to comply with these regulations.

The significance of this statutory declaration and the consequences of a false statutory declaration under criminal law (Sections 156, 161 of the German Criminal Code) are known to me.”

Date Signature

Declaration of own contribution

Yiyi Ji contributed the following to the below publication:

Publication 1: **Ji Y**, Hoffmann W, Pham M, Dunn AE, Han H, Oezerdem C, Waiczies H, Rohloff M, Endemann B, Boyer C, Lim M, Niendorf T and Winter L, “High peak and high average radiofrequency power transmit/receive switch for thermal magnetic resonance.” Magn. resonance in medicine (2018). DOI: 10.1002/mrm.27194.

Contribution:

- Researched the literature
- Understanding the current state of the art
- Development of the study concept/protocol
- Design concepts for high-frequency transmit/receive hardware for RF heating and MRI at 7.0 Tesla
- Construction, characterization, evaluation, and application of high power transmit/receive switch
- Primary data acquisition
- Data analysis and its critical interpretation
- Creation of diagrams and figures
- Writing and revising the manuscript

_____

Signature, date and stamp of first supervising university professor / lecturer

_____

Signature of doctoral candidate

Journal Data Filtered By: **Selected JCR Year: 2017** Selected Editions: SCIE,SSCI Selected Categories: **"RADIOLOGY, NUCLEAR MEDICINE and MEDICAL IMAGING"** Selected Category Scheme: WoS

Gesamtanzahl: 128 Journale

Rank	Full Journal Title	Total Cites	Journal Impact Factor	Eigenfactor Score
1	JACC-Cardiovascular Imaging	8,104	10.247	0.026360
2	European Heart Journal-Cardiovascular Imaging	4,630	8.336	0.020640
3	EUROPEAN JOURNAL OF NUCLEAR MEDICINE AND MOLECULAR IMAGING	14,983	7.704	0.024870
4	RADIOLOGY	54,109	7.469	0.063710
5	JOURNAL OF NUCLEAR MEDICINE	27,101	7.439	0.037560
6	CLINICAL NUCLEAR MEDICINE	4,756	6.281	0.006950
7	INVESTIGATIVE RADIOLOGY	6,486	6.224	0.012410
8	Circulation-Cardiovascular Imaging	5,438	6.221	0.020160
9	IEEE TRANSACTIONS ON MEDICAL IMAGING	17,837	6.131	0.024200
10	ULTRASOUND IN OBSTETRICS & GYNECOLOGY	12,420	5.654	0.018820
11	INTERNATIONAL JOURNAL OF RADIATION ONCOLOGY BIOLOGY PHYSICS	46,595	5.554	0.055060
12	JOURNAL OF CARDIOVASCULAR MAGNETIC RESONANCE	4,918	5.457	0.013530
13	NEUROIMAGE	92,719	5.426	0.152610
14	MEDICAL IMAGE ANALYSIS	6,383	5.356	0.011900
15	RADIOTHERAPY AND ONCOLOGY	17,184	4.942	0.027840
16	HUMAN BRAIN MAPPING	20,334	4.927	0.042810
17	SEMINARS IN NUCLEAR MEDICINE	2,285	4.558	0.002990
18	ULTRASCHALL IN DER MEDIZIN	2,201	4.389	0.004310
19	MAGNETIC RESONANCE IN MEDICINE	31,440	4.082	0.034130
20	EUROPEAN RADIOLOGY	18,615	4.027	0.034120
20	SEMINARS IN RADIATION ONCOLOGY	2,480	4.027	0.003620
22	JOURNAL OF NUCLEAR CARDIOLOGY	3,508	3.847	0.004120
23	AMERICAN JOURNAL OF NEURORADIOLOGY	22,667	3.653	0.029840
24	JOURNAL OF MAGNETIC RESONANCE IMAGING	16,398	3.612	0.027440
25	MOLECULAR IMAGING AND BIOLOGY	2,415	3.608	0.005480

Publication

Ji Y, Hoffmann W, Pham M, Dunn AE, Han H, Oezerdem C, Waiczies H, Rohloff M, Endemann B, Boyer C, Lim M, Niendorf T and Winter L, “High peak and high average radiofrequency power transmit/receive switch for thermal magnetic resonance.” Magn. resonance in medicine (2018).

https://doi.org/10.1002/mrm.27194

Curriculum Vitae

My curriculum vitae does not appear in the electronic version of my paper for reasons of data protection.

List of Publications

Original peer-reviewed publications:

1. **Ji Y**, Winter L, Navarro L, Ku MC, Periquito J, Pham M, Hoffmann W, Theune L, Calderon M, Niendorf T, “Controlled Release of Therapeutics from Thermoresponsive Nanogels: A Thermal Magnetic Resonance Feasibility Study.” *Cancers* **2020**, *12*, 1380. doi: 10.3390/cancers12061380.

2. Periquito J, Paul K, Huelnhagen T, Ku M-C, **Ji Y**, Cantow K, Gladytz T, Grosenick D, Flemming B, Seeliger E, Waiczies S, Niendorf T, Pohlmann A, “Diffusion-weighted renal MRI at 9.4 Tesla using RARE to improve anatomical integrity.” Scientific reports, 2019, 9.1: 1-12. https://doi.org/10.1038/s41598-019-56184-6.

3. **Ji Y**, Hoffmann W, Pham M, Dunn AE, Han H, Oezerdem C, Waiczies H, Rohloff M, Endemann B, Boyer C, Lim M, Niendorf T and Winter L, “High peak and high average radiofrequency power transmit/receive switch for thermal magnetic resonance.” Magn. resonance in medicine (2018). DOI: 10.1002/mrm.27194.

4. Niendorf T, Oezerdem C, **Ji Y**, Oberacker E, Kuehne A, Waiczies H and Winter L, “Radiative RF antenna arrays for cardiac, brain and thermal magnetic resonance at ultrahigh and extreme magnetic field strengths: Concepts, electromagnetic field simulations and applications.” In Electromagnetics in Advanced Applications (ICEAA), 2017 International Conference on (pp. 1567-1570). IEEE. DOI: 10.1109/ICEAA.2017.8065585.

5. Winter L, Oberacker E, Paul K, **Ji Y**, Oezerdem C, Ghadjar P, Thieme A, Budach V, Wust P, and Niendorf T, "Magnetic resonance thermometry: methodology, pitfalls and practical solutions." International Journal of Hyperthermia 32, no. 1 (2016): 63-75. DOI: 10.3109/02656736.2015.1108462.

6. Waiczies S, **Ji Y**, Niendorf T. "Chapter 11 Fluorinated Natural Compounds and Synthetic Drugs" Fluorine Magnetic Resonance Imaging, Ed. Ulrich Flögel, Ed. Eric Ahrens, Pan Standford Publishing, 2016. DOI: 10.1201/9781315364605-12

7. Winter L, Oezerdem C, Hoffmann W, van de Lindt T, Periquito J, **Ji Y**, Ghadjar P, Budach V, Wust P and Niendorf T, "Thermal magnetic resonance: physics considerations and electromagnetic field simulations up to 23.5 Tesla (1GHz)." Radiation Oncology 10, no. 1 (2015): 201. DOI: 10.1186/s13014-015-0510-9.

8. Winter L, Oberacker E, Oezerdem C, **Ji Y**, von Knobelsdorff-Brenkenhoff F, Weidemann G, Ittermann B, Seifert F and Niendorf T, “On the RF Heating of Coronary Stents at 7.0 Tesla MRI”. Magnetic resonance in medicine 74, no. 4 (2015): 999-1010. DOI: 10.1002/mrm.25483.

9. **Ji Y**, Waiczies H, Winter L, Neumanova P, Hofmann D, Rieger J, Mekle R, Waiczies S and Niendorf T, "Eight-channel transceiver RF coil array tailored for

1H/19F MR of the human knee and fluorinated drugs at 7.0 T." NMR in Biomedicine 28.6 (2015): 726-737. DOI: 10.1002/nbm.3300.

10. Lepore S, Waiczies H, Hentschel J, **Ji Y**, Skodowski J, Pohlmann A, Millward JM, Paul F, Wuerfel J, Niendorf T and Waiczies S, “Enlargement of Cerebral Ventricles as an Early Indicator of Encephalomyelitis”, PLoS One 8, no. 8 (2013): e72841. DOI:10.1371/journal.pone.0072841.

Conference abstracts:

1. **Ji Y**, “RF induced release of a load from a thermoresponsive nanocarrier: a thermal magnetic resonance study”, 10th Annual scientific Symposium on Ultrahigh Field Magnetic Resonance, Berlin, Germany, 2019. Invited oral presentation. **Awarded best oral presentation prize (rising star)**.
2. **Ji Y**, Hoffmann W, Pham M, Dunn AE, Niendorf T and Winter L, “Radio frequency heating induced release of a fluorescent model drug attached to a thermoresponsive polymer carrier: A 7.0 T thermal MR study”, joint MDC/FMP PhD retreat Groß Dölln, Templin, Germany, 2017. Oral presentation. **Awarded best oral presentation prize (3rd place)**.
3. **Ji Y**, Hoffmann W, Pham M, Dunn AE, Niendorf T and Winter L, “Radio frequency heating induced release of a fluorescent model drug attached to a thermoresponsive polymer carrier: A 7.0 T thermal MR study”, 8th Annual scientific Symposium on Ultrahigh Field Magnetic Resonance, Berlin, Germany, 2017. Poster presentation and power pitch. **Awarded best poster prize (3rd place)**.
4. **Ji Y**, Hoffmann W, Pham M, Han H, Oezerdem C, Waiczies H, Niendorf T and Winter L, “High peak and high average RF power transmit/receive switch for an integrated RF heating applicator operating at 297 MHz (7.0 Tesla)”, 8th Annual scientific Symposium on Ultrahigh Field Magnetic Resonance, Berlin, Germany, 2017. Poster presentation.
5. **Ji Y**, Hoffmann W, Pham M, Oezerdem C, Waiczies H, Niendorf T, and Winter L, “Higher is better: High peak and high average RF power transmit/receive switch for an integrated RF heating applicator operating at 297 MHz (7.0 Tesla)”, 25th Annual meeting of International Society of Magnetic Resonance in Medicine, Honolulu, Hawaii, USA, 2017. E-poster presentation.
6. **Ji Y**, Dunn A, Pham M, Hoffmann W, Ku MC, Waiczies H, Waiczies S, Boyer C, Lim M, Niendorf T, and Winter L, “Detailing radio frequency heating induced release of a fluorescent model drug attached to a thermoresponsive polymer carrier: A 7.0 T thermal MR study”, 25th Annual meeting of International Society of Magnetic Resonance in Medicine, Honolulu, Hawaii, USA, 2017. E-poster presentation.

7. **Ji Y**, Hoffmann W, Pham M, Oezerdem C, Winter L, Niendorf T, et al., “High Power Transmit/Receive Switch for Thermal MR at 7.0 Tesla.”, 7th Annual Scientific Symposium on Ultrahigh Field Magnetic Resonance, Berlin, Germany, 2016. Poster Presentation.

8. **Ji Y**, Hoffmann W, Winter L, Oezerdem C, Niendorf T, “High Power Transmit/Receive Switch for Thermal MR at 7.0 Tesla.” Int. Soc. Magn. Res. Med. workshop on UHF MRI, Heidelberg, Germany, 2016. Poster presentation.

9. **Ji Y**, Waiczies H, Winter L, Neumanova P, Hofmann D, Rieger J, Mekle R, Waiczies S, and Niendorf T, “Eight Channel Tx/Rx RF Coil Array for 1H/19F MR of the Human Knee and Fluorinated Drugs at 7.0 T”, 6th Annual Scientific Symposium on Ultrahigh Field Magnetic Resonance, Berlin, Germany, 2015. Poster Presentation.

10. **Ji Y**, Waiczies H, Winter L, Neumanova P, Hofmann D, Rieger J, Mekle R, Waiczies S, and Niendorf T, “Eight Channel Tx/Rx RF Coil Array for 1H/19F MR of the Human Knee and Fluorinated Drugs at 7.0 T”, 23rd Annual meeting of International Society of Magnetic Resonance in Medicine, Toronto, Canada, 2015. Poster presentation.

Acknowledgments

I want to thank my supervisors Prof. Thoralf Niendorf and Dr. Lukas Winter from the Berlin Ultrahigh Field Facility (B.U.F.F.) at the Max-Delbrück Center for Molecular Medicine in the Helmholtz Association for their enthusiasm, encouragement, guidance, and support.

I want to thank my co-supervisor Prof. Peter Wust from Charité – Universitätsmedizin Berlin for his availability, kindness and support.

I want to thank all my colleagues and friends from B.U.F.F. specially João Periquito, Min-Chi Ku, Leili Riazy, Eva Peper, Eva Oberacker and Celal Özerdem for all the support, helpful discussions, companionship, shared moments of stress and laughter.

I want to thank Dr. Werner Hoffmann from Physikalisch-Technische Bundesanstalt Berlin, from whom I learnt so much about MR hardware.

I want to thank my collaborators Alex Dunn, Dr. May Lim and Dr. Cyrille Boyer from New South Wales University, Australia and Dr. Lucila Navarro, Dr. Neha Tiwari and Prof. Marcelo Calderón from Freie Universität Berlin. Without their work on smart nanocarriers, this thesis wouldn’t be complete.

I want to thank my family and friends Ji Zhengrong, Xia Weifen, Pusheng Ji, Tiago Silva, Carolina Galvão, Carolina Fontinha and Raquel Fernando for their amazing support in the stressful moments; they always land me a hand and pulled me through.